Aus der Chirurgischen Klinik
der Medizinischen Fakultät Mannheim
(Direktor: Prof. Dr. med. Christoph Reißfelder)

Potential Therapeutic Effect of Human Adipose-Derived Stem Cells

on hypoxia *in vitro* and *in vivo*

Inauguraldissertation
zur Erlangung des medizinischen Doktorgrades
der
Medizinischen Fakultät Mannheim
der Ruprecht-Karls-Universität
zu
Heidelberg

vorgelegt von
Jiaxing Zheng

aus
Xinjiang, China
2021

Dekan: Prof. Dr. med. Sergij Goerdt
Referent: Prof. Dr. med. Felix Rückert

CONTENTS

ABBREVIATIONS

Table 1. List of abbreviations used in this study.

Activating transcription factor 4	ATF4
Activating transcription factor 6	ATF6
Adipose stem cells	ASCs
AMP-activated protein kinase)	AMPK
Angiotensin-converting enzyme	ACE
Ankle-brachial index	ABI
Atherosclerosis-prone apolipoprotein E-deficient	ApoE$^{-/-}$
B-cell lymphoma 2	Bcl-2
Binding immunoglobulin protein	BIP
c-Jun N-terminal kinases	JNK
Cardiovascular disease	CVD
Cobalt (II) chloride	CoCl$_2$
Critical limb ischemia	CLI
cytoplasmic ROS	cytoROS
Cyan fluorescent protein	CFP
Desferrioxamine	DFO
DNA damage-inducible transcript 3	CHOP

Double ligation of the femoral artery	DFLA
Double-stranded RNA-dependent protein kinase (PKR)-like ER kinase	PERK
Endoplasmic reticulum	ER
Endoplasmic-reticulum-associated protein degradation	ERAD
Endothelial cells	ECs
Endothelium Nitric oxide synthase	eNOS
Eukaryotic Initiation Factor 2	eIF2
Femoral nerve	FN
Femoral vein	FV
Fetal bovine serum	FBS
Gastrocnemius muscles	GM
glucose transporter 1	GLUT1
Growth arrest and DNA damage-inducible protein	GADD43
Hypoxia-inducible factor 1-alpha	HIF-1a
Immunofluorescence	IF
Immunohistochemistry	IHC
Inositol-requiring enzyme 1α	IRE1α
Intermittent claudication	iC
Mesenchymal stem cells	MSCs
Myocardial infarction	MI
NADPH oxidase	NOX

Nitric oxide	NO
Paraformaldehyde	PFA
Peripheral Artery Disease	PAD
phingosine-1-phosphate	S1P
phingosine-2-phosphate	S1P
Pluripotent stem cells	IPSCs
Reactive oxygen species	ROS
Regulated Ire1-dependent decay	RIDD
Sarcoplasmic/endoplasmic reticulum Ca^{2+} ATPase	SERCA2a
Spermatogonial stem cells	SPCs
Superficial femoral artery	FA
Unfolded protein response	UPR
Vascular endothelial growth factor	VEGF
Vastus Laterals	VL
Von Willebrand factor	VWF
X-box binding protein 1	XBP1
Yellow fluorescent protein	YFP

1 INTRODUCTION

1.1 Definition of PAD and Epidemiology

Peripheral artery disease, also known as peripheral arterial disease (PAD), is a chronic circulatory disease characterized by narrowed arteries and reduced blood flow to the limbs[1-4]. A hallmark of PAD is endothelial cell (EC) dysfunction caused by atherosclerosis (AS) or plaque formation in the peripheral blood vessels in the extremities, consequently leading to tissue ischemia[4-6]. Although PAD commonly affects the legs, it is also a systemic disease with diverse clinical manifestations including ischemic heart disease, stroke, abdominal aortic aneurysm formation, and other severe medical conditions. The mild form of PAD either is asymptomatic or results in intermittent claudication (IC), whereas severe PAD is associated with critical limb ischemia (CLI), characterized by rest pain, ischemic ulceration, foot gangrene, myocardial infarction (MI), stroke, and limb loss[6-13]. PAD is diagnosed based on a patient's medical history and physical examination. In addition, ankle–brachial index (ABI) is used to assess the severity of the disease[14].

With more than 10% of patients with PAD in their 60s and 70s, age plays a crucial role in its prevalence[15,16]. Furthermore, the incidence of PAD is expected to rise in the future due to an increase in the global aging population. PAD shares several risk factors with cerebrovascular and coronary artery disease, such as smoking, diabetes, obesity, and hypertension[17]. Moreover, after

adjusting for known cardiovascular disease (CVD) risk factors, PAD was found to be associated with an increased incidence of cerebrovascular and coronary heart disease and mortality[17,18]. CLI, the most severe pattern of PAD, is associated with a 6-month mortality rate of 20% and a 5-year mortality rate of 50%[16-18]. In addition, CLI is associated with a high risk of lower limb amputation in approximately 10 to 40% of patients[19,20].

1.2 PAD Treatment

With the number of elderly individuals estimated to reach 1.5 billion in 2050[21], efficient diagnostic methods and better treatment options are necessary for PAD management. Treatment strategies should aim at reducing both the symptoms and related cardiovascular events and PAD progression. Changes in lifestyle, risk factor management, exercise, drug intervention, and surgical revascularization play a pivotal role in improving a patient's condition[22-24].

The conservative treatment approach involves the use of medications to improve ambulatory activity and modify risk factors for patients. For example, pentoxifylline promotes tissue oxygenation and improves the blood flow to the affected area[24-26]. Angiotensin-converting enzyme (ACE) inhibitors trigger anti-atherosclerotic effects by increasing nitric oxide (NO) release and inhibiting the degradation of bradykinin[26-28]. Similarly, prostaglandin decreases pain and promotes healing in patients with severe limb ischemia[31-33].

Surgery is indicated for patients in advanced stages and who can safely tolerate it[18,19,24]. Revascularization approaches such as femoral-popliteal bypass

grafting or endovascular revascularization using balloon angioplasty and stenting and thrombendarteriectomy and sympathectomy are performed to relieve symptoms, heal ulcers, prevent amputations and improve the quality of life[28-31]. However, amputation could be considered for uncontrolled infections, rest pain, and progressive gangrene without the option of revascularization. Recently, stem cell therapy has emerged as a non-invasive treatment approach, especially for diabetic patients with PAD, because it reduces the extent of trauma to the affected limb and may alleviate rest pain.

1.3 Stem Cell Therapy

Regenerative medicine using therapeutic stem cells has emerged as an alternative strategy, especially for patient's ineligible for revascularization procedures, to improve the blood supply to ischemic area[26,27]. Stem cells are classified as

–totipotent cells that can form all kinds of extraembryonic tissues, e.g., zygote.

–pluripotent cells that can generate all kinds of body cells including germ cells, e.g., embryonic stem cells (ESCs), induced pluripotent stem cells (iPSCs), i.e. inner cell mass of the blastocyst;

–multipotent cells that possess the ability to form all kinds of tissue cells, e.g., tissue stem cells such as mesenchymal stem cells (MSCs);

–unipotent cells that can form only a single cell type, e.g., spermatogonial stem cells (SPCs)[41].

The most abundantly used stem cells in regenerative medicine are MSCs because they can be easily cultured and expanded. Adipose-derived stem cells (ASCs) are mesenchymal stem cells (MSCs) that are obtained from abundant adipose tissue, adherent on plastic culture flasks, can be expanded in vitro, and have the capacity to differentiate into multiple cell lineages.

1.4 Clinical Use of ASCs

Adipose stem cells (ASCs) were first identified and isolated in 2001 and have been used in 187 clinical trials[27,28]. Since 2007, there has been a tremendous increase in the use of ASCs in human clinical trials, which reached its peak in 2015. In addition, six trials were registered on ClinicaTrials.gov in the first quarter of 2019. ASCs have recently been used for treating bone diseases, respiratory diseases, skin diseases, neurological diseases, autoimmune diseases, diabetes, and lung and heart diseases[33-35]. ASCs are enzymatically isolated from the stromal vascular fraction of adipose tissue[27] and can be directly injected into the wound or blood. Furthermore, ASCs can be encapsulated in biological material and implanted into the wound[35-38]. Several studies have shown that ASCs can increase the cure rate and reduce the cure time both *in vivo* and *in vitro*[35-37]. These benefits could be attributed to ASC properties such as rapid differentiation into specific cell lineages, including keratinocytes, fibroblast-like cells, and endothelial cells (EC); and release of cytokines and growth factors to promote angiogenesis, development, and

fibroblast migration and production[38-40]. Stem cell therapy using ASCs has also been extensively used to treat Peripheral artery disease (PAD)[26-31]. At present, the therapeutic potential of Adipose-derived stem cells has been tested in a small number of patients with PAD. After the injection of ASCs, the patient's pain score scale and claudication walking distance have been significantly improved[117].

1.5 Therapeutic Mechanisms of ASCs

ASCs exert their therapeutic effects via cell migration to the site of tissue damage and differentiation[30-33]. Their ability to migrate is highly significant if the lesion is widely distributed or when the damaged tissue is inaccessible[30-33]. Their ability to repair and regenerate, differentiate into several different cell lineages, secrete bioactive soluble factors, promote angiogenesis, and anti-apoptotic activity further contribute to their therapeutic benefits[31-33]. In addition, the anti-inflammatory effect of ASCs protects the organism by reducing the severity of the inflammatory immune response[34]. ASCs exert their anti-apoptotic activity by inhibiting the programmed cell death via paracrine signaling to preserve the organ function[38]. They can secrete antibacterial peptides, such as Lipocalin-2 and LL-37, in response to pathogen stimuli[39-41]. Soluble factors secreted by ASCs improve tissue vascularity by stimulating endothelial cells (ECs) to promote new angiogenesis and growth. ASCs improve the vascularization in injured tissues by inducing the expression of angiogenic cytokines such as vascular endothelial growth factor (VEGF)[28,33,34].

1.6 Role of Hypoxia in inducing Angiogenesis under PAD

Vessel occlusion observed in PAD is commonly caused by the formation of atherosclerotic plaques. Atherosclerosis initiates with the deposition of lipid deposits below the vascular endothelium which triggers an inflammatory response[42]. The build-up of plaques may partially occlude the blood vessels and obstruct the blood flow, resulting in tissue ischemia and hypoxia. Tissue hypoxia increases the production of reactive oxygen species (ROS)[9] like hydrogen peroxide, superoxide, and peroxynitrite[43-45]. Cytoplasmic ROS (cytoROS), is produced as a by-product of PAD in the pathological conditions[44-46]. The NADPH oxidase (NOX) family of enzymes are responsible for generating cytoROS. During angiogenesis in ECs, the NOX-dependent ROS production induces the expression of hypoxia-inducible factor 1α (HIF1α)-mediated glucose transporter 1 (GLUT1) expression, hexokinase activity, and resultant glycolysis in response to low oxygen tension[42-45].

Other sources of cytoROS are nitric oxide synthases (eNOS [endothelium], nNOS [neuronal], and iNOS [inducible]). CytoROS induces the activity of AMP-activated protein kinase (AMPK) that regulates cell metabolism including glycolysis, lipid metabolism, mitochondrial function, cell growth, and autophagy[44-46].

Blood vessels trigger adaptive responses, including angiogenesis, to restore blood flow to injured tissue. Angiogenesis, first identified by Folkman in the 1970s, is the process of developing microvessels from pre-existing vessels

either via sprouting angiogenesis or intussusception[42]. Angiogenesis is primarily driven by hypoxia, during which the ECs deliver oxygen and nutrients to the ischemic tissue and synthesize new capillaries. In addition, hypoxia increases the expression of several genes, including HIF-1[45-48] that augments the transcription of genes involved in ischemic vascular remodeling, cell proliferation, and mobilization of bone marrow-derived cells and proangiogenic factors such as VEGF and eNOS[46-48.]

1.7 Calcium and ROS

Calcium acts as a second messenger to regulate numerous cell functions, including cell survival and cell death. In the mitochondria, ROS are produced as a by-product of mitochondrial respiratory chain activity. The crosstalk between ROS and calcium signals is bidirectional, wherein ROS regulate calcium signaling and the latter is implicated in ROS production Figure 1. Under normal circumstances, Ca^{2+} reduces the mitochondrial ROS production. However, under hypoxia, abundant cytoplasmic Ca^{2+} is pumped into the endoplasmic reticulum (ER) lumen by sarcoplasmic/endoplasmic reticulum Ca^{2++} ATPase (SERCA2a) to promote the production of ROS. Furthermore, eNOS-produced NO stimulates cytosolic Ca^{2+} uptake by SERCA2a. Excessive accumulation of ROS, which can ensure normal angiogenesis, causes cell apoptosis to maintain calcium homeostasis under mitochondrial regulation. Disruption of calcium–ROS balance at the SR/ER-mitochondrial interface has been implicated in several diseases[48-53].
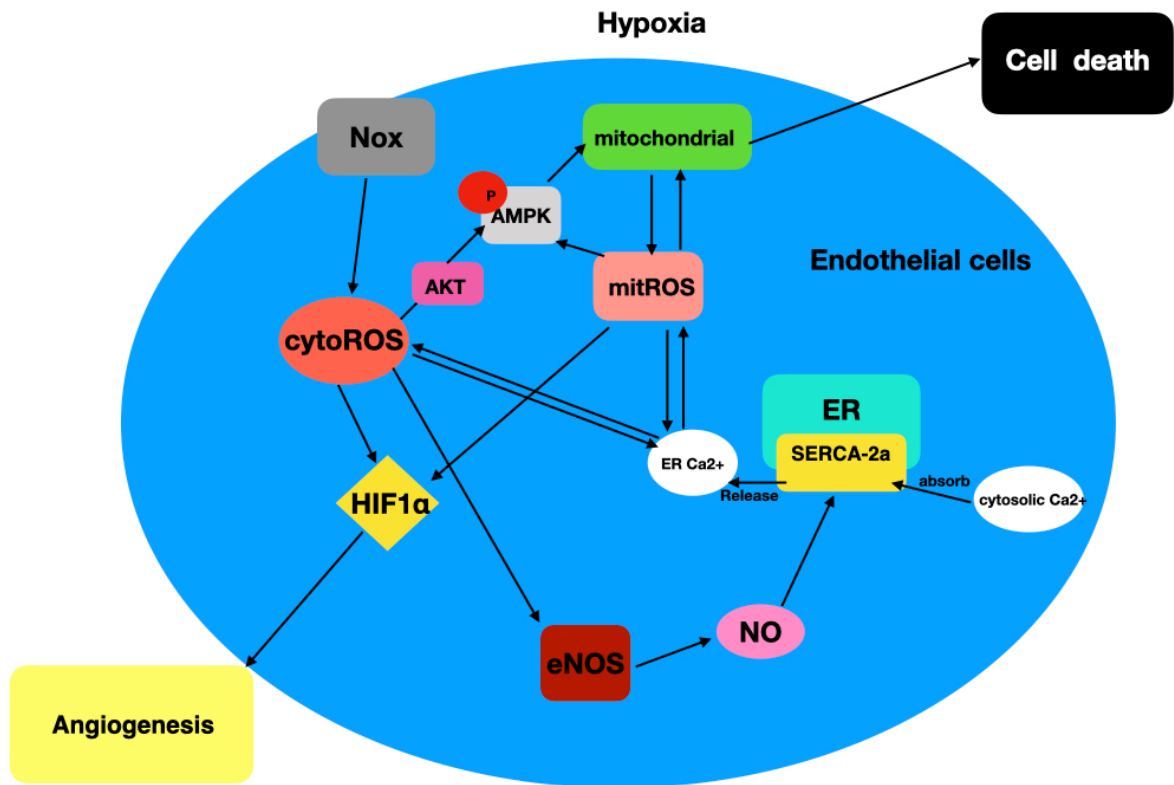
Figure 1. Schematic representation of angiogenesis under hypoxia and role of different factors. Under hypoxic conditions, endothelial cells produce high levels of mitochondrial ROS and cytoROS, resulting in two effects. Firstly, excessive accumulation of ROS activates the AMPK activity by inducing its phosphorylation. This initiates the mitochondrial apoptosis program, resulting in the death of numerous endothelial cells. Secondly, ROS increases the expression of HIF1a, promoting angiogenesis in endothelial cells under hypoxia. During this process, maintaining the intracellular calcium balance of calcium ions reaches a critical point, including the endoplasmic reticulum (ER) storage and release of calcium ions into the cytoplasm, regular transport of extracellular calcium ions, and the release of eNOS. Thus, cells can better transmit the signals and regulate the calcium ion conductivity of SERCA2a.

1.8 ER Stress and Unfolded Protein Response

The endoplasmic reticulum (ER) is involved in multiple cellular activities, including synthesis, maturation, translation, and folding of secretory and membrane proteins; lipid biogenesis; and Ca^{2+} homeostasis. Hypoxia triggered by physiological stressors[50] disrupts the calcium homeostasis and induces dysfunction of ER and protein folding. Consequently, the accumulation of numerous misfolded proteins in the ER lumen generates ER stress. Eukaryotic cells have evolved an unfolded protein response (UPR) to ensure the fidelity of protein folding and prevent the accumulation of unfolded or misfolded proteins. UPR alters a cell's transcriptional and translational programs to solve the protein-folding defect and restore normal ER functions[51]. Mammalian cells recruit three UPR signaling cascades, initiated by three ER-localized protein sensors: inositol-requiring enzyme 1α (IRE1α), double-stranded RNA-dependent protein kinase (PKR)-like ER kinase (PERK), and activating transcription factor 6 (ATF6)[85-87]. Under normal physiological conditions, these sensors are associated with abundant ER chaperone BiP (immunoglobulin-heavy-chain-binding protein; also known as HSPA5 and GRP78) and remain inactive. Their activation reduces the accumulation of unfolded proteins and accelerates the rate of protein folding in the ER lumen. The downstream transcriptional programs of the UPR act to restore proteostasis. IRE1α increases the protein-folding capacity of ER, assists in endoplasmic-reticulum-associated protein degradation (ERAD), and limits the entry of new protein

molecules (regulated Ire1-dependent decay [RIDD])[85-87]. PERK induces the transcription of genes and escapes translation inhibition under ER stress. ATF6 increases the ER capacity to activate transcriptional programs and direct the misfolded proteins for degradation (ERAD). UPR-induced genes include those that increase the protein-folding capacity of the ER and mediate its expansion by increasing the biogenesis of ER and lipid components. However, if restoration of proteostasis fails and ER stress is unabated, the UPR signaling switches to a pro-apoptotic mode, a process known as the terminal UPR. The terminal UPR may have evolved to eliminate, for example, excessively damaged or pathogen-infected cells. It is believed that study of ROS and calcium ions under hypoxia, and ER stress can provide a further understanding of these interactions in relation to several diseases, including PAD Figure 2.
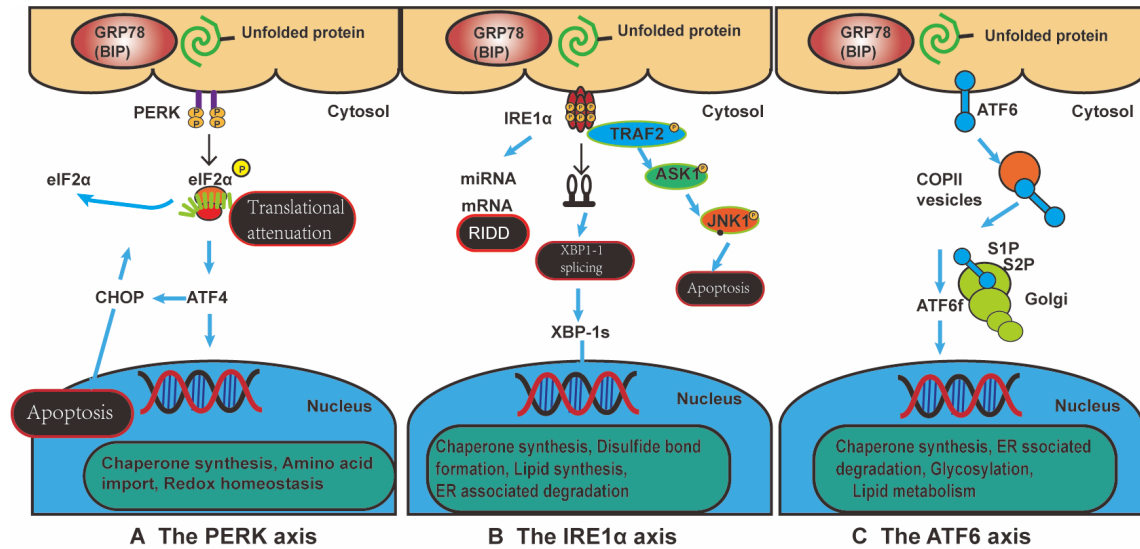
Figure 2. UPR signal pathway. Three sensors located at the ER membrane mediate the ER stress response: IRE1α, ATF6 and PERK. Accumulation of unfolded protein recruits BiP to the ER lumen and its dissociation from IRE1α, ATF6 and PERK leads to their activation. Upon dimerization and autophosphorylation, IRE1α splices XBP-1 mRNA, which adjusts the reading frame to allow translation of an active transcriptional factor XBP-1. XBP-1 up-regulates UPR genes encoding ER chaperones and components of the ERAD machinery. IRE1α can also recruit TRAF2 and ASK1, leading to downstream activation of c-Jun N-terminal kinases (JNK) and p38 MAPK. Activated JNK translocates to the mitochondrial membrane and promotes (a) activation of Bim and (b) inhibition of B-cell lymphoma 2 (Bcl-2), whereas p38 MAPK phosphorylates and activates DNA damage-inducible transcript 3(CHOP). PERK phosphorylates Eukaryotic Initiation Factor 2 (eIF2α) and attenuates protein translation. However, translation of selected mRNAs is favored under these conditions, including Activating transcription factor 4 (ATF4), which then induces expression of CHOP and growth arrest and DNA damage-inducible protein (GADD34). Activated ATF6 translocates to the Golgi, where its cytosolic domain is cleaved by the proteases, Sphingosine-1-phosphate (S1P) and Sphingosine-2-phosphate (S2P). The cleaved ATF6 fragment forms an active transcriptional factor that mediates expression of several components important for protein folding, degradation, and ER expansion. It was made using adobe illustrator 2021

1.9 Aims of the study

This thesis aims to explore the therapeutic mechanism of adipose derived stem cells for a PAD model *in vitro* and *in vivo*, which can be divided into the following two parts:

In vitro:

1. To establish an appropriate cell culture environment to simulate hypoxia.

2. Investigate the expression of HIF-1a in endothelial cells under hypoxia.

3. To investigate the effects of stem cells and stem cell conditioned media on endothelial cells under hypoxia in terms of angiogenesis.

4. To examine the effect of hypoxia on HUVECs kept in coculture with ASCs.

5. To detect calcium changes in the cytoplasm and endoplasmic reticulum under hypoxic conditions.

6. Investigate the expression of the ER stress sensors (BIP, XBP1, CHOP, ATF6) in endothelial cells under hypoxia.

In vivo:

1. To establish PAD ApoE$^{-/-}$ Mouse model to simulate acute limb ischemia.

2. The effect of stem cells on lower extremity arterial obstruction was evaluated and analyzed based on following parameters:

    - capillary density via immunohistochemistry

    - the survival rates

    - HE is staining of the gastrocnemius muscle

    - plasma detection of Cholesterol, Triglycerides, and Creatine Kinase

- muscle imaging under a light-sheet microscope, and via

- expression of ER stress sensors (BIP, XBP1, CHOP, ATF6).

2 MATERIALS AND METHODS

2.1 Material

2.1.1 Cell Culture Products

Table 2. List of cells used in this study.

Product	Company	Catalog No.
Adipose-derived mesenchymal stromal cells (ASC)	Self-isolated; Mannheim Ethics Commission II (2009-210N-MA).	
Human umbilical vein endothelial cells (HUVEC)	Self-isolated; Mannheim Ethics Commission II (2015-518N-MA)	
Human umbilical vein endothelial cells (HUVEC)	ATCC	CRL-1730

Table 3. List of cell culture reagents used in this study.

Product	Company	Catalog No.
NB6 GMP grade collagenase	SERVA Electrophoresis	17458
Collagenase	Gibco	17100017
EDTA	Applichem	A3145,0500
DMEM (glucose 1g/L)	PAN Biotech	P04-01500
DMEM (no glucose)	PAN Biotech	P04-01549
Pooled human allogeneic serum from AB donors (AB serum)	German Red Cross Blood Donor Service, Institute Mannheim	
Penicillin/Streptomycin	PAN Biotech	P06-07100
L-glutamine	PAN Biotech	P04-80100

Product	Company	Catalog No.
D-glucose	Sigma-Aldrich	G7021
Endothelial cell basal medium (EBM)	PromoCell	C-22011
Supplement Mix endothelial cell growth medium 2	PromoCell	C-39216
Pericytes Growth Medium	PeloBiotech	PB-MH-0314000
Speed Coating Solution	PeloBiotech	PB-LU-000-0002-00
Trypsin/EDTA	PAN Biotech	P10-024100
Fetal Bovine Serum	Sigma	F7524
Dimethylsulfoxide (DMSO)	Wak-Chemie Medical GmbH	WAK-DMSO-10
Ficoll-Paque™ Premium	GE Healthcare Bio-science AB	17-5442-03
DPBS (1X)	Gibco	14190-094
Albumin fraction V (bovine serum albumin)	Carl Roth	8076.2
N-Acetylcysteine (NAC)	Sigma	A9165
WZB-117 (3-hydroxy-benzoic acid, 3- fluoro-1,2-phenylene) ester	Cayman Chemicals	19900
Speed Coating Solution	PeloBiotech	PB-LU-000-0002-00
DPBS (1X)	Gibco	14190-094
Paraformaldehyde (PFA)	Roth	0335.3
Triton x100	Sigma Aldrich	23,472-9
Albumin fraction V (bovine serum albumin)	Carl Roth	8076.2
DAPI	Sigma	1.24653
Mounting medium	ibidi	50001

Product	Company	Catalog No.
L-Kynurenine	Santa Cruz	Sc-202688
Trichloroacetic acid	Roth	8789.2
para-Dimethylaminobenzaldehyde	Santa Cruz	Sc202888
Acetic acid	J.T.Baker	6052
DPBS	Gibco	14190-094
Tween-20	Serva	37470.01
Albumin Fraction V (bovine serum albumin)	Roth	8076.2
Color Reagent A (H_2O_2)	R&D Systems	DY999
Color Reagent B (Tetramethylbenzidine)	R&D Systems	DY999
2N H_2SO_4 (ELISA Stop solution)	Sigma	1.60313

2.1.2 Antibodies

Table 4. List of antibodies used in this study.

Product	Clone	Species	Type	Company	Catalog No.
Anti human-alpha smooth muscle actin	Polyclonal	Mouse	Monoclonal IgG_{2a}	PROGEN	65001
GRP78(BIP)	Polyclonal	Rabbit	IgG	Invitrogen	PA5-34941
XBP1	Polyclonal	Rabbit	IgG	Invitrogen	PA5-27650
ATF6	Polyclonal	Rabbit	IgG	Invitrogen	PA5-20215

Product	Clone	Species	Type	Company	Catalog No.
ATF6	Polyclonal	Mouse	IgG	Novusbio	NBP1-40256SS
Phospho-IRE1 alpha	Polyclonal	Rabbit	IgG	Invitrogen	PA1-16927
IRE1 alpha	Polyclonal	Rabbit	IgG	Invitrogen	PA1-16928
GADD153(CHOP)	Polyclonal	Mouse	IgG	Novusbio	NB600-1335
Beta-actin	Polyclonal	Mouse	IgG	Abcam	ab8227
Anti-mouse-Alexa Fluor 488 F(ab')$_2$	Polyclonal	Goat	IgG, IgM (H+L)	Invitrogen	A10684
Mouse anti-rabbit	Polyclonal	Mouse	IgG-HRP	Santa-curz	Sc2357
m-IgGκ BP-HR	Polyclonal	Rabbit	m-IgGκ BP	Santa-curz	Sc516102

2.1.3 Consumables

Table 5. List of plastic consumables used in this study.

Product	Company	Catalog No.
96-well cell culture plate	Eppendorf	0030 790.119
24-well cell culture plate	Thermo Fisher	142475
12-well cell culture plate	Thermo Fisher	150628
6-well cell culture plate	Thermo Fisher	140675

Product	Company	Catalog No.
Transwell inserts (pore size 0.4 µm transparent ThinCerts-TC inserts)	Greiner bio-one	657641
175 cm^2 cell culture flasks	Thermo Fisher	159910
25 cm^2 cell culture flasks	Thermo Fisher	156367
96-well black cell culture plate	Perkin Elmer	6005550
8-well µ-slide	ibidi	80826
Petri dish	Corning	353803
50 ml Cell star tubes	Greiner bio-one	188271
15 ml Cell star tubes	Greiner bio-one	227261
1000 µl sterile filter tips	SurPhob	VT0263X
200 µl sterile filter tips	SurPhob	VT0243X
10/20 µl sterile filter tips	Star Lab	S1120-3710
10 ml PD sterile tips	Brand	631060
5 ml PD sterile tips	Brand	702390
2.5 ml PD sterile tips	Brand	702388
1.25 ml PD sterile tips	Brand	702386
25 ml serological sterile pipettes	Star Lab	190105-071
10 ml serological sterile pipettes	Star Lab	180720-070
5 ml serological sterile pipettes	Star Lab	180806-069

2.1.4 Laboratory equipment

Table 6. List of equipment used in this study

Device	Name	Provider
Centrifuge	5810R	Eppendorf
Centrifuge	5920R	Eppendorf
Cell counter	Nucleo Counter	Chemometec
Plate washer	Well wash 4MK2	Thermo Fisher
Small Centrifuge	Minispin	Eppendorf
Microscope	Axiovert 100	ZEISS
Microscope Camera	AxioCam M Rc	ZEISS
Microscope	SP5	Leica
Microscope	SP8	Leica
Microscope	Standard 25	Zeiss
Laminar flow hood	Hera safe	Thermo Fisher
Chemical flow hood	Airflow-Control EN14175	Caspar and Co. Labora
Microplate reader	TECAN infinite M200PRO	Tecan
Microplate reader	Spark	Tecan
Pipettes	Research plus (0.5-2.5µl)	Eppendorf
Pipettes	Research plus (1-10µl)	Eppendorf
Pipettes	Research plus (1-200µl)	Eppendorf
Pipettes	Research plus (1-1000µl)	Eppendorf
Trans-Blot Turbo Transfer Sys.	TSGP15D	Biorad

2.1.5 Software for Data Analysis

Table 7. List of software used in this study.

Software	Version	Company
FlowJo	10	FlowJo, LLC, Ashland, OR, USA
FlowJo	7	FlowJo, LLC, Ashland, OR, USA
GraphPad Prism	8	GraphPad Software Inc. San Diego, USA
ImageJ	1.5	NIH
i-Control	1.10	TECAN
LEGENDplex™ Data Analysis Software	8.0	BioLegend
FCAP Array Software	3.0	BD
IncuCyte S3 software	S3	Essen BioScience, Ltd.
SPSS	19.0	IBM
AutoCellSeg[115]		Developed by Bioinformaticians at the research group of Prof. Gretz.

2.2 Methods

2.2.1 Cell Lines and Cell Culture

Human umbilical vein endothelial cells (HUVECs) were isolated from different donor human umbilical cords, provided by the Obstetrics Department of the University Hospital Mannheim. HUVECs isolation was approved by the local ethics committee (Medizinische Ethik-Kommission II, Medizinische Fakultät Mannheim, 2015-581N-MA, Mannheim, Germany). The detailed isolation protocol has been described earlier[62]. HUVECs were cultured in endothelial cell growth medium (2011101, Provitro, Germany) containing 5% fetal bovine serum (FBS) and 1% penicillin and streptomycin in 1% gelatin-coated culture flasks. Immunofluorescence (IF) assays were used to identify and validate HUVECs. The cells showed positive staining for CD31, von Willebrand factor (vWF), and VE-cadherin, which are specific markers for ECs. HUVECs (self-isolated) and HUVECs (procured from ATCC) were simultaneously compared via doubling time experiment. Division of Vascular Surgery, Department of Surgery, University Hospital Mannheim, provided the adipose tissue for isolation of ASCs. ASCs isolation from donor adipose tissue was approved by the local ethics committee (Medizinische Ethik-Kommission II, Medizinische Fakultät Mannheim, 2009-210N-MA, Mannheim, Germany). The identification and isolation of ASCs were performed by the laboratory of Prof. Dr. Karen Bieback. Frozen cells were thawed in low glucose Dulbecco's modified Eagle

medium (P0404515, Pan Biotech, Germany) containing 10% FBS, 1% penicillin and streptomycin, and 1% L-glutamine. ASCs and HUVECs were incubated at 37C° in a humidified incubator with 5% CO_2 and 95% humidity. The medium was changed every 2 days. HUVECs and ASCs were used between second to fifth passages of in all experiments.

2.2.2 ASC Treatment

Stem cell treatment methods *in vitro* constituted co-culture of ASCs with HUVECs (ASC-CO) and treatment of HUVECs with ASC-conditioned medium (ASC-CM). For ASC co-culture, 0.6×10^4 ASC/cm^2 were seeded into ThinCert™ cell culture inserts suitable for 6- and 24-well plates (657640 and 657640, Greiner Bio-One, Germany). Next, 2×10^4 $HUVECs/cm^2$ were inoculated in 6- and 24-well plates coated with gelatin, respectively, as previously described[63-69]. The ASC-CM was prepared as previously reported[69] and frozen at $-80°C$ for later use. Stem cell treatment *in vivo* was delivered by intramuscular injection of ASC cells, as described previously[62].

2.2.3 Chemically Induced Hypoxia Cell Models

To create an EC hypoxia model, cobalt (II) chloride ($CoCl_2$) was used. To test the appropriate concentrations of $CoCl_2$ in HUVECs, the following preliminary experiments were performed:

(1) Effect of 4h $CoCl_2$ on viability of HUVECs was measured via methyl thiazolyl-phenyl-tetrazolium bromide (MTT) assay (see Methods section 2.1.5 MTT measurement)

(2) Western blotting (WB) was performed to detect HIF-1α expression in HUVECs (see Methods section 2.1.11 Western blotting)

(3) ROS signaling from ECs that were transduced with redox-sensitive green fluorescent protein 3 (roGFP3) was studied (see section 2.1.10 Plasmid and Method Transduction).

For dose–response experiments, 10 µM, 25 µM, 100 µM, 125 µM, and 500 µM of CoCl$_2$ concentrations were used. For kinetics–response experiments, HUVECs were treated with CoCl$_2$ for 1 h, 4 h, 8 h, and 24 h. Regression analysis was performed to determine the HUVEC viability, HIF-1α expression, and ROS levels by calculating the EC$_{50}$ value.

2.2.4 Doubling Time Assay

Endothelial cells were grown in the endothelial cell culture medium. The cells were passaged at a ratio of 1:3. Cells were seeded in a 6-well plate, each well containing 8×10^4 cells, and the experiment duration was 120 h. The cell density in the two wells was calculated every 24 h and a cell growth curve was drawn to calculate the doubling time. The calculation formula used was:

$$Doubbling\ time = duration * \frac{\log(2)}{[\log(final\ cell\ concentration) - \log(initial\ cell\ concentration)]}$$

2.2.5 MTT assay

The MTT (M2128, Sigma, American) assay was performed to detect cell viability. 4×10^4 HUVECs in the log phase were collected and seeded on

collagen-coated 24-well plates (1.9 cm^2) or 96-well plates. One-day post seeding cells were treated with CoCl$_2$, ASC-CM, and ASC-CO. After 24 of treatment, MTT dye solution (1mg/ml in HUVECs medium) was given to the cells for 4h. Next, the formazan salt crystals were dissolved in 100 µL of MTT solvent, which contained 40% of Dimethyl sulfoxide (DMSO, HN47.1, Roth, Germany), 40% of 10%-sodium dodecyl sulfate (SDS, 0183.3, Roth, Germany), 20% of DPBS, and 1.2% of Acetic acid (6755.1, Roth, Germany).The absorbance was read the next day at 540 nm (reference length 630 nm) using a multi-mode microplate reader (Spark, Switzerland).

2.2.6 Scratch Assay

Endothelial cells were seeded into 12-well plates, each well containing 1×10^5 cells. After overnight incubation, cells in different experimental groups were treated with CoCl$_2$, ASC-CM, and ASC-CO for 4 h. After the treatment, a single, straight layer was scraped using a 200 µL pipette tip and images were acquired using a camera attached to an inverted microscope (DM IRB; Leica, Berlin, Germany) at 0 h, 3 h, 6 h, 12 h, and 24 h. The gap was quantitatively evaluated using the AutoCellSeg[115]. All the experiments were performed thrice with two technical replicates and HUVECs from three different donors.

2.2.7 Tube Formation

A tube formation assay was performed in HUVECs using the method described earlier[72]. After 4 h of treatment with CoCl$_2$, cells were diluted with 1% FBS medium to 2.5×10^4 cells/mL. Next, the cells were seeded into pre-coated 24-

well plates (10,000 cells/well) in a Matrigel basement membrane matrix without phenol red (356237, Corning, USA). After 4h $CoCl_2$ treated, HUVEC was then respectively treated with ASC-CM or ASC-CO. Then 6 h of incubation, images were acquired using an inverted microscope and analyzed using the Angiogenesis Analyzer software plugin for NIH ImageJ. All the experiments were performed thrice with two technical replicates and HUVECs from three different donors.

2.2.8 Plasmids and Transduction

To measure the dynamic changes in ER Ca^{2+} and ROS signaling in HUVECs, self-inactivating recombinant lentiviruses encoding pPM337-D1ER and roGFP3 were used to achieve a high transduction efficiency in the cultured cells[72,73]. D1ER, a genetically encoded and ratiometric ER Ca^{2+} biosensor, containing enhanced YFP (excitation 514 nm/emission 527 nm) and CFP (excitation 430 nm/emission 474 nm), was synthesized by Genewiz from Merck Sigma-Aldrich in pUC57 with XbaI and BamHI restriction sites. The sequence of D1ER published by Addgene (https://www.addgene.org/36325/) was used for synthesis. pUC57-D1ER was further cloned into pPM337 via XbaI and BamHI restriction sites and used for generating virus particles. As both the flurosecnt proteins are expressed in ratio of 1:1 in the sensor and binding of Calcium causes change in the conformation of the D1ER leading to fluorescence resonance energy transfer (FRET), ratiometric FRET, which is

calculated by dividing Emission (Em) $_{CFP}$ by Em $_{YFP}$. It reflected the dynamic changes in ER Ca^{2+} concentration.

RoGFP3 [Excitation 395 nm Emission 528 nm / Excitation 485 nm Emission 528 nm] is a redox indicator that can track changes in ROS levels both in the mitochondrial matrix and cytosol under oxidizing conditions. The sequence of Grx1-roGFP3 was kind gift from Dr. Manfred Frey (Steinbeis-Innovationszentrum Zellkulturtechnik, University of Applied Sciences, Mannheim). Grx1-roGFP3 was synthesized via GENWIZ service from Sigma Aldrich and cloned into pHR'SIN-cPPT-SEW (Demaison et al., 2002) via restriction sites BamHI and XbaI.

The lentivirus was produced as described previously[24,25].

To transduce the sensors into HUVECs, 0.5×10^6 log-phase cells were pre-cultured in a T25 flask. HUVECs were transduced with either 50 μL of recombinant lenti-virus particles expressing the roGFP3 or D1ER mixed with the fresh medium at a confluency of 40 to 60% confluency. Three passages after transduction or 72 hours post transduction (after daily washes with 10ml PBS and Medium change) cells were used for further experiments.

2.2.9 Measurement of ER Calcium

To detect the dynamic changes in the ER Ca^{2+}, HUVECs transduced with the D1ER sensor were seeded into a 24-well plate (3.8×10^4 cells per well). The cells were first treated with 80 μM $CoCl_2$ for 4 h, followed by treatment with ASC-CM and ASC-CO for 24 h. In parallel, the fluorescence intensity of CFP

(Cyan fluorescent protein) and YFP (Yellow fluorescent protein) was detected using a multi-mode microplate reader every 2 h.

In addition, HUVECs transduced with the D1ER sensor were seeded into a 15 mm cover glass coated with 1% gelatine a 24-well plate (3.8 × 104 cells per well). The cells were subsequently treated with 80 µM CoCl2 (each treatment included three groups). Next, the cells were treated with ASC-CM and ASC-CO for 24 h. After treatment, the cells were washed thrice with cold Dulbecco's phosphate-buffered saline (DPBS) and subsequently fixed with 4% paraformaldehyde (PFA). Finally, after washing thrice with cold DPBS, the sample was fixed with a drop of a mounting medium. The SP5 microscope system (Leica, Germany) was used to detect the YFP and CFP fluorescence. The images were analyzed using the NIH ImageJ software to compare the fluorescence intensity between different groups. All the experiments were performed thrice with two technical replicates and HUVECs from three different donors.

2.2.10 Measurement of Cytoplasmic Calcium

Ratio metric calcium indicator dye Fura-2 was used for cytoplasmic calcium measurement in HUVECs. To this end, HUVECs were seeded into 24-well plates with 8×10^4 cells per well, The cells were incubated with 3 µM Fura-2-pentakis (acetoxymethyl) ester (Fura-2 AM, 50033, Biotium) for 60 min, and subsequently washed twice with HBSS (5.4 mmol/L KCl, 136 mmol/L NaCl, 0.34 mmol/L Na_2HPO_4, 0.44 mmol/L KH_2PO_4, 5.6 mmol/L D-glucose, and 80 µM $CaCl_2$ (pH 7.4). Next, the cells were treated with $CoCl_2$, ASC-CM, and ASC-

CO 24h. The dynamic changes in cytoplasmic Ca^{2+} were studied by detecting the fluorescence of Fura-2 AM by a multimode microplate reader every 2 h (excitation: 340 nm/380 nm; emission: 535 nm) and using ImageJ software (340 nm/380 nm).

2.2.11 Measurement of ROS Levels

HUVECs (3.8×10^4) transduced with roGFP3 were seeded into a 24-well plate. Next, HUVECs were treated with 80 µM $CoCl_2$ for 4 h. Afterward, the cells were treated with ASC-CM and ASC-CO for 24 h. The dynamic changes in the fluorescence intensity of roGFP3 were monitored using a multi-mode microplate reader at two excitations - 395 nm and 485 nm and emission at 510 nm. The ratio of emission (395 nm/485 nm) was calculated and plotted over time. The oxidation of the roGFP3-Grx redox sensor results in an increase in the emission fluorescence at 528 nm when excited at 485 nm and a decrease in emission fluorescence when excited at 395 nm.

2.2.12 Apoptotic Assay

HUVECs were divided into control and test groups and seeded into T25 flasks. When the cells reached 60% confluency, they were treated with 80µM $CoCl_2$ 4h. The positive control was treated with staurosporine. After 4 h of treatment, the cells were harvested and processed according to protocol and manufacturer's guidelines (FITC Annexin V Apoptosis Detection Kit with PI 640914, BioLegend). The cells were placed in FACS tubes, sorted, and

processed using the FACS machine (CantoTM II, BD, USA). The data were analyzed using FlowJo (BD, New York, USA).

2.2.13 Ethics and Animals

All experiments were approved by the Regional Government authority (G-239/18, Regierungspräsidium Nordbaden, Karlsruhe Germany), and agreed with the EU guidelines 2010/63/EU. All experiments were performed according to the EU guidelines 2010/63/EU for the Care and Use of Laboratory Animals. Male ApoE$^{-/-}$ mice with the C57BL/6J background were purchased from Charles River Laboratories. A lower limb arterial ischemia model was established, and the therapeutic potential of ASCs was evaluated using 24 mice. The mice were divided into control and treatment groups, each with 12 mice and were fed a Western diet (5% cholesterol and 21% fat) for 12 weeks from the age of 8 weeks. Four animals were placed in a cage before the surgery, and each animal was placed in a separate cage after the surgery to prevent the mice from fighting. Mice in the control group were treated with normal saline, and those in the treatment group were administered stem cell therapy (

Table *8*). All animals received analgesics after the surgery (described in **section 2.2.14 Anesthesia and Surgery**), and mice were evaluated daily after the surgery.

Table 8. Division of mice in experimental groups.

Group	Animal number	Treatment
Control	12	Saline
Treatment	12	ASCs

2.2.14 Anesthesia and Surgery

In a day, four mice of a group were operated, sequentially. Anesthesia was performed using a combination of medetomidine, midazolam, and fentanyl (MMF)[74]. Midazolam (5 mg/kg), medetomidine (0.05 mg/mL/kg), and fentanyl (0.5 mg/kg) were mixed in equal proportion, and subsequently 0.05 g/mL of the mix was subcutaneously injected into the mouse. After 6 minutes of anesthesia, when mouse breathed slowly and stably, hairs on their lower limbs were removed using a depilatory cream (Veet, France). A saline solution was injected subcutaneously to maintain sufficient fluid in the body. Next, the mouse was placed on a 37°C heating pad and the skin was rubbed with an alcohol scrub. An incision of about 3 to 4 mm was made in the middle of the groin area using pointed tip forceps and surgical scissors. To increase the surgical field of view, all surgical procedures were performed under a dissecting microscope (Axiovert 100, ZEISS, Germany). The superficial femoral artery (FA) was dissected from the femoral vein (FV) and femoral nerve (FN). The FA was ligated proximally and distally and excised. Then the wound was ligated at the distal end of the FA to suture the wound.

Immediately after the surgery, 100 µL of ASCs (1×10^8 cells/mL), prepared by the Experimental Cell Therapy Laboratory (Prof. Karen Bieback), was injected into five different muscle positions (20 µL each). After the surgery, the mouse was placed in a clean cage on a heating pad, and their breathing and heartbeat were continuously monitored. Subsequent injections were followed by rehydration with normal saline. When the mouse was mobile, subcutaneous injections of buprenorphine was administered. The mouse was returned to its cage, vital signs were re-evaluated every 4 h. All animals received Buprenorphine sc (0.1 mg/kg body weight every 8 hours for first 24 h postoperatively) for pain management. Analgesia was followed by the administration of Metamizole in the drinking water (24 mg metamizole/5ml water corresponding to a dose of 200 mg/kg 4 times daily).
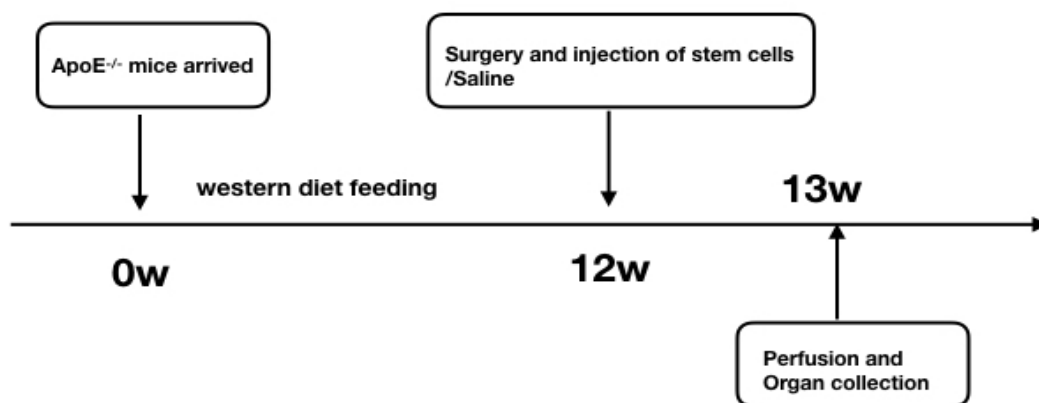
Figure 3. Timeline for *in vivo* experiment. Mice were fed a Western diet (5% cholesterol and 21% fat) for 12 weeks. At week 12, mice were operated on, and at week 13, 100 µL of normal saline and ASCs were injected into the control and ASC treatment groups.

2.2.15 Plasma and Organ Collection

Blood samples were collected from the ophthalmic venous plexus (orbital sinus) under anesthesia in lithium-heparinized tubes using capillaries for blood collection. After centrifugation at 2000 g for 5 min at 4°C, the plasma was collected in 1.5 mL tubes and stored at −80°C until further analyses. Mice were administered anesthesia, fresh vastus lateralis (VL) was quickly removed from both sides before immersing it in 4% PFA. Next, the bilateral GM was immediately excised, following which the organs and tissues were obtained quickly and kept at 4°C for further analyses.

2.2.16 Histological Evaluation

Histological analysis of ischemic and non-ischemic hindlimb GM was performed on all mice by H&E staining and IHC(Immunohistochemistry). Muscle samples were fixed in 4% PFA, embedded in paraffin, and cut into thin slices (3–4 μm). The sections were stained with H&E. In addition, an anti-CD31 antibody (1: 200, Abcam, ab28364) was used for IHC staining to assess microvessel density. ImageJ was used to calculate the percentage of the microvascular area (CD31-positive area) in five randomly selected fields of view (×40). To estimate the plaque burden in the blood vessels, the abdominal aorta was removed, fixed overnight in 4% PFA, and embedded in paraffin, followed by excision into 4-μm thick sections. To determine AS in the arteries, the sections were stained with H&E, and the progression of AS lesions was measured as previously described[79] (Table 9).

Table 9. Classification of AS.

	Appearance
Early-stage	Cell-rich foam but lacking a necrotic core.
Moderately advanced	Containing a fibrotic cap and often a necrotic core but no medial macrophage infiltration.
Advanced lesion	Medial macrophage infiltration, elastic lamina degradation, and pronounced necrosis and fibrosis.

AS: atherosclerosis.

2.2.17 LDH Assays

LDH is a ubiquitous enzyme among vertebrate organisms which catalyzes the reversible conversion of pyruvate to lactate, with concomitant conversion of Nicotinamide adenine dinucleotide (NADH) and Nicotinamide adenine dinucleotide (NAD+). The concentration in the skeletal muscle represents the level of glycolysis[90]. The relative levels of LDH in the VL tissue were detected according to the manufacturer's guidelines from the LDH kit (ab197000, Abcam, Germany). Briefly, the 40mg tissue was homogenized tissue using a T18 digital homogenizer (IKA, USA) at the highest speed of 25,000 rpm for 30 s prior to keep on ice for 10 min. Then, tissue lysate was subsequently centrifuged for 5 min at 4°C at 10,000 x g the supernatant was then collected and added into 96-well-plate (50 µl each well). Hereafter, 50 µl reaction mix supplied by the kit was

added into each sample. Then the fluorescence intensity at 535/587 nm (Ex/Em) was immediately measured by a multimode microplate reader.

2.2.18 Myoglobin ELISA Assay

Myoglobin (Mb) is cytoplasmic protein present in oxidized skeletal muscle fibers that promotes the delivery of oxygen during conditions of high metabolic oxygen demand. Thus, it reflects the level of skeletal muscle regeneration and aerobic respiration following an ischemic injury. The relative level of Mb in the VL tissue was detected using the Mb kit (ab210965, Abcam, Germany) according to the manufacturer's instructions. Firstly, the 40 mg gastrocnemius muscle tissue was homogenized tissue using a T18 digital homogenizer (IKA, USA) at the highest speed of 25,000 rpm for 30 s prior to keep on ice for 10 min. Next, 50 µL of tissue lysate supernatant was added to each well of a 96-well plate that was incubated at room temperature for 1 h. After washing with wash buffer, 100 µL of 3,3',5,5'-tetramethylbenzidine developing solution was added to each well. The plate was incubated for 10 min. Finally, the stop solution (50 µL per well) was added, and the optical density was measured at 450 nm on a multi-mode microplate reader.

2.2.19 Plasma Detection

To determine the postoperative levels of cholesterol, triglycerides, and creatine kinase (CK) in mice, 100 µL of plasma per mouse was collected in a 1.5-mL Falcon tube. All plasma samples were analyzed at Zentrum für Medizinische Forschung at the Medical Faculty Mannheim, University of Heidelberg, using a

Cobas c 311 Analyzer (Roche, Switzerland) according to the manufacturer's manual and guidelines.

2.2.20 Western Blotting

Western blotting (WB) was performed to detect the protein expression. Protein (mixed with loading buffer [161-0767, Bio-Rad, Germany]) isolated from HUVECs and mice hindlimb muscle tissue was denatured by incubation at 100°C for 10 min. The denatured protein (15–20 µg) was loaded onto 10% SDS-PAGE gels and electrophoresed at 200 V for about 35 min. Next, the proteins were transferred onto polyvinylidene fluoride (PVDF, 1620177, Bio-Rad, Germany) membranes. Hereafter, the PVDF membranes were blocked for 1 h in Tris-buffered saline with 0.1% Tween 20 (TBST) containing 5% non-fat milk. Membranes were next incubated overnight at 4°C with primary antibodies against GRP78 (BIP) (1:5000, PA5-34941, Invitrogen, USA), XBP1 (1:1000, PA5-27650, Invitrogen, USA), ATF6 (1:1000, PA5-20215, Invitrogen, USA), ATF6 (1:1000, NBP1-40256SS, Novus Biologicals Germany), GADD153 (CHOP) (1:1000, NB600-1335, Novus Biologicals), phospho-IRE1 alpha (1:1000, PA1-16927, Invitrogen, USA), IRE1 alpha (1:1000, PA1-16928, Invitrogen, USA), and β-actin (1:1000, ab8227, Abcam, Germany). After the incubation with primary antibodies, PVDF was washed thrice with TBST (10 min each time) and incubated for 1 h at room temperature with corresponding horseradish peroxidase (HRP)-conjugated anti-rabbit (Sc-2357, 1:1000, Santa Curz, Germany) or anti-mouse (Sc-51610, 1:1000, Santa Curz) secondary

antibody. The membrane was washed again thrice with TBST (5 min each), following the detection of the immune reactive protein bands using an enhanced luminol reagent (western lightning，203-19251，China) and visualized by chemiluminescence (1 to 5-min exposure). For detecting the phosphorylation of IRE1 alpha, the PVDF membrane was stripped using the following protocol: the stripping buffer with 2-mercaptoethanol (M6250, Sigma-Aldrich, USA) was heated to 65°C, PVDF membrane was immersed in the stripping buffer for 35 min with agitation. The PVDF membrane was washed extensively for 10 min in TBST twice. After washing the membrane, it was blocked for 1 h in TBST containing 10% non-fat milk. After stripping, the PVDF membrane was incubated with primary and secondary antibodies and subsequently exposed as described earlier. Densitometric analysis was performed using the NIH ImageJ software (v1.52, Bethesda, USA).

2.2.21 Statistical Analysis

Statistical analyses were performed using SPSS 19.0 (IBM Corp., Armonk, USA) and GraphPad Prism 8 (GraphPad, USA). Results of different experimental groups are expressed as mean ± SD. The EC_{50} and IC_{50} values of $CoCl_2$ were determined using a regression analysis performed using GraphPad Prism 8. The differences between the groups were analyzed by one-way or two-way analysis of variance (ANOVA), followed by Tukey's post hoc correction analysis and χ^2 test. The experimental readouts from MVD, LDH, Mb,

CK, and protein expression were normalized to the left hindlimb (non-ischemic

side) for each mouse. A *p*-value < 0.05 was considered statistically significant.

3 RESULTS

3.1 Results From *in vitro* Experiments

3.1.1 Identification of Endothelial cells

ECs were obtained using a previously described method[62]. To confirm their identity, the HUVECs were compared with commercially obtained HUVECs (purchased from ATCC) for morphology, growth curve, and cell migration. Isolated ECs expressed specific markers, CD31, vWF, and VE-cadherin, as confirmed by immunofluorescence staining (Figure 4a). These results showed that the isolated HUVECs were morphologically similar to commercially derived ECs. While comparing the doubling time of HUVECs with that of ATCC cells, the results revealed no significant differences (Figure 4b). We simultaneously counted the cells every day for 120 h to obtain a cell growth curve. After comparing with ATCC HUVECs, the results showed no significant difference (Figure 4c). MTT assays performed at different cell densities revealed no significant differences in cell viability and their metabolic activities between isolated HUVECs and ATCC HUVECs (Figure 4d). Next, we closely observed the migratory ability of both cells. All cells filled the gap within 24 h. A comparison of the cell migration area of the two groups of cells after 12 h revealed no significant difference (Figure 4e). These results showed that HUVECs were morphologically and functionally identical to ATCC ECs and did not affect the overall experiment when used in *in vitro* hypoxia model. To further reduce the error in the experiment, we randomly mixed and grouped the three

41

different donor cells and performed experiments with two technical replicates and three repetitions with different passages.
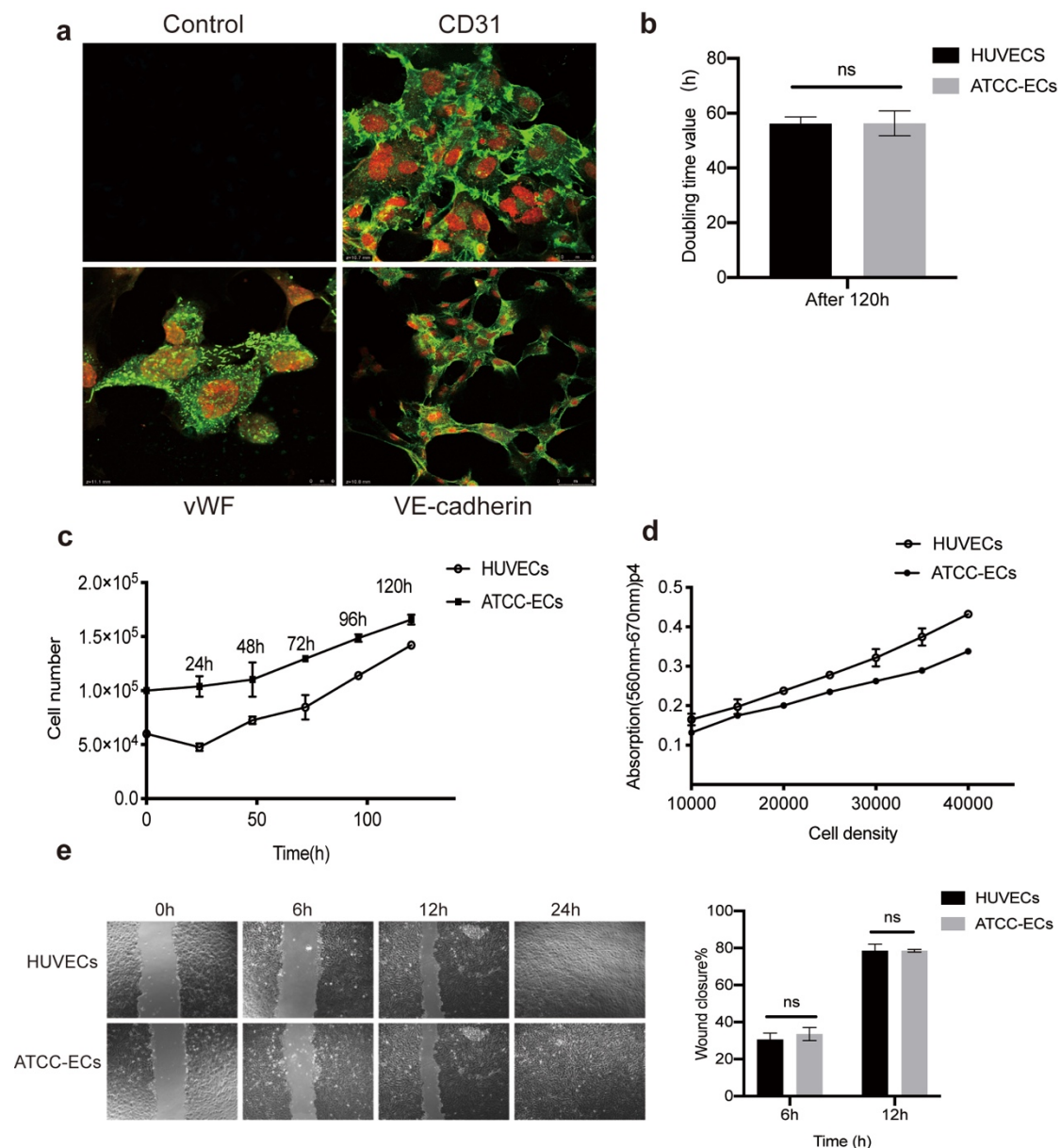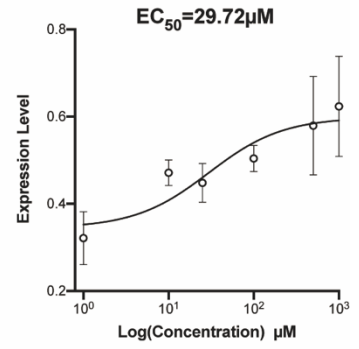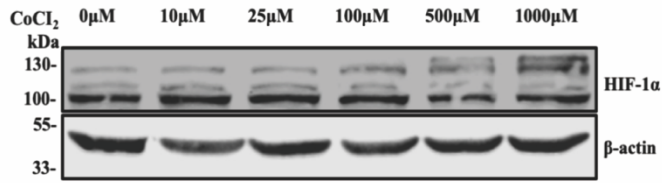

Figure 4 Identification of human umbilical vein endothelial cells (a) Immunofluorescence of HUVEC cells. The control group, the self-isolated HUVECs did not show a change in the expression of CD31, vWF, and VE-cadherin., confirming that the cells were endothelial cells (scale bar is 10 μm). **(b)** A comparison of isolated HUVECs and ATCC HUVECs for doubling time did not reveal significant differences. **(c)** A comparison of growth curves of HUVECs and ATCC cells did not reveal significant differences. **(d)** A comparison of MTT assays did not reveal a significant difference between the two groups of cells. **(e)** A comparison of the migration area of cells after 9 h and 12 h in the cell scratch assay revealed no significant difference between the two groups of cells. (ns, not significant, scale bar is 500 μm).

3.1.2 CoCl$_2$ based in-vitro hypoxia model

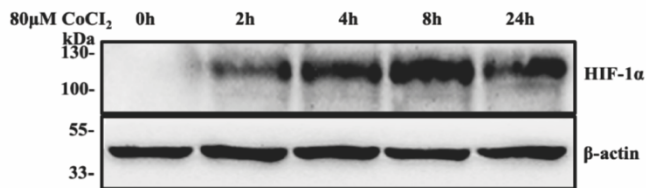CoCl$_2$ is widely used to mimic a hypoxic environment. CoCl$_2$ generates a hypoxic environment by strongly stabilizing HIF-1α and HIF-2α[78,79]; Co^{2+} in CoCl$_2$ competitively replaces Fe^{2+} in prolyl hydroxylase (PHD), a key enzyme that links O$_2$ concentration to HIF degradation[79-81]. The WB results indicated that the expression of HIF-1α increased with increasing concentration of CoCl$_2$. The EC$_{50}$ of CoCl$_2$ concentration was 29.72 µM (Figure 5a). HIF-1α expression displayed time-dependent characteristics. CoCl$_2$ treatment for ≥ 4 h significantly increased its expression (Figure 5b). Apoptosis was assessed using propidium iodide (PI) and Annexin V staining followed by flow cytometry. After 4 h of treatment, 80 µL of CoCl$_2$ was compared with staurosporine(1µg/µl). A significant difference was found between CoCl$_2$ and the positive control group (staurosporine), with no significant differences compared with the control group (Figure 5c, d). Moreover, we did not find a difference in cell necrosis, apoptosis, and survival between the CoCl$_2$-treated and control groups. However, a significant difference between CoCl$_2$ and the positive control groups was observed (Figure 5 e). The results showed that HUVECs did not undergo extensive apoptosis after CoCl$_2$ treatment for 4 h. HUVECs treated with different concentrations of CoCl$_2$ showed a dose-dependent increase in ROS levels. (Figure 5 f, g). The cell migration experiment showed that HUVECs under hypoxia migrated slowly (Figure 5 h). These results demonstrated that CoCl$_2$ induced a hypoxic environment.
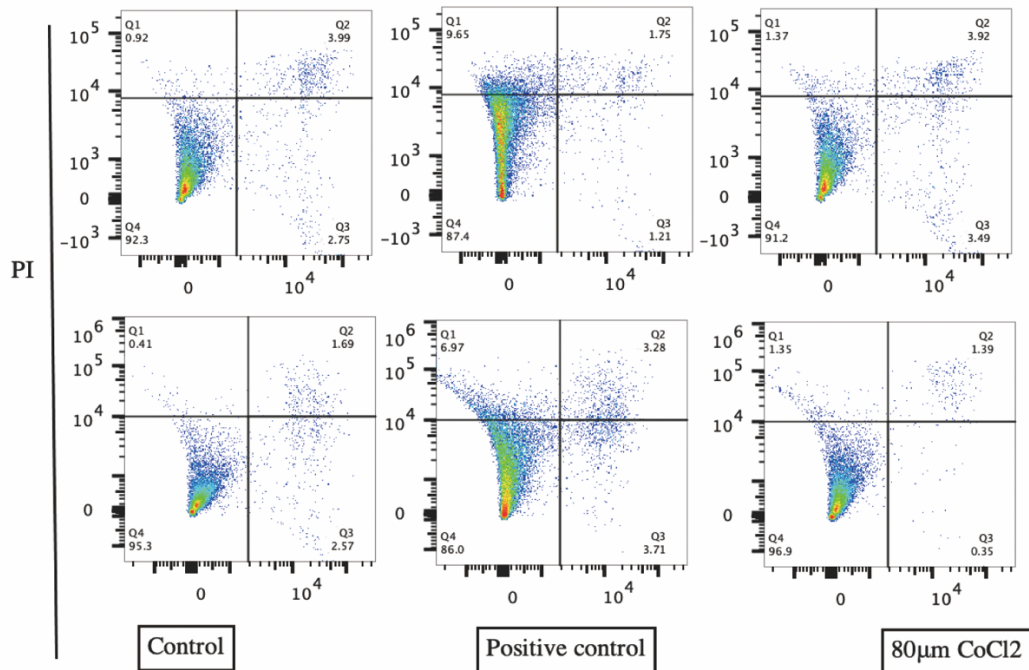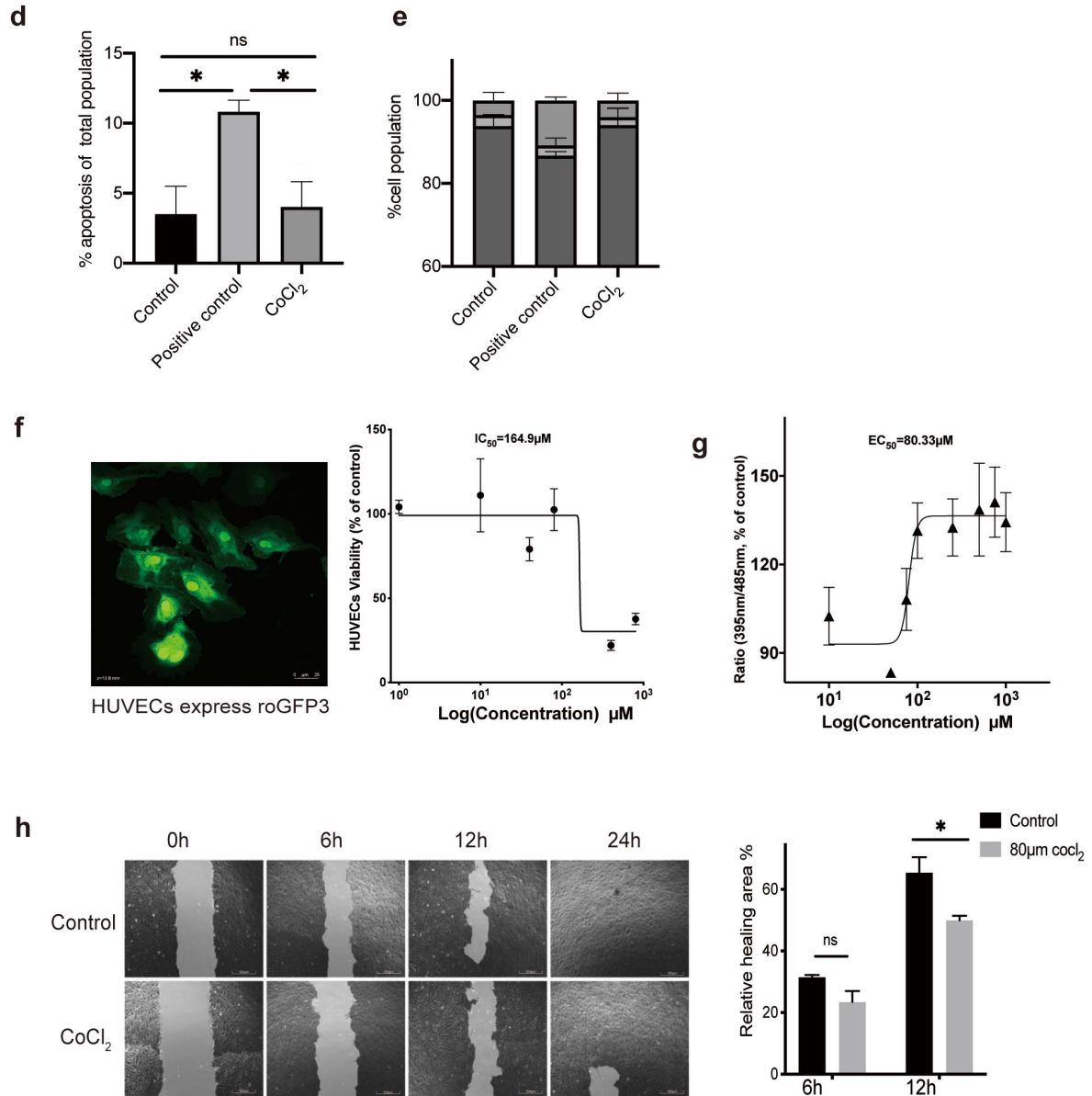
a

CoCl₂ 0μM   10μM   25μM   100μM   500μM   1000μM
kDa
130-
100-   HIF-1α
55-
33-   β-actin

$EC_{50}=29.72\mu M$

Expression Level
0.8
0.6
0.4
0.2
10^0 10^1 10^2 10^3
Log(Concentration) μM

b

80μM CoCl₂   0h   2h   4h   8h   24h
kDa
130-
100-   HIF-1α
55-
33-   β-actin

Expression Level
2.0
1.5
1.0
0.5
0.0
*   *   ns
0h   2h   4h   8h   24h
Time (h)

c

PI

Q1 0.92   Q2 3.99   Q1 9.65   Q2 1.75   Q1 1.37   Q2 3.92
Q4 92.3   Q3 2.75   Q4 87.4   Q3 1.21   Q4 91.2   Q3 3.49

Q1 0.41   Q2 1.69   Q1 6.97   Q2 3.28   Q1 1.35   Q2 1.39
Q4 95.3   Q3 2.57   Q4 86.0   Q3 3.71   Q4 96.9   Q3 0.35

Control   Positive control   80μm CoCl2

Annexin V

44

Figure 5 CoCl$_2$ induces hypoxic environment (a) Treatment with CoCl$_2$ increased the expression of HIF-1α in a dose-dependent manner. Regression analysis revealed an EC$_{50}$ value of 29.72 μM. (b) The expression of HIF-1α increased in a time-dependent manner following treatment with CoCl$_2$. Treatment for ≥4 h significantly increased its expression. (c) FACS result of PI and Annexin V (d) Fluorescent staining using PI and Annexin V to compare the number of apoptotic cells revealed no difference between CoCl$_2$ and control groups. (e) A significant difference was observed when comparing the treatment groups to the positive control group. (f) The viability of RoGFP3-expressing HUVECs decreased with the increase in CoCl$_2$ concentration. Regression analysis of HUVEC viability indicated a CoCl$_2$ IC$_{50}$ of 164.9 μM (scale bar is 10 μm). (g) Regression analysis also indicated that CoCl$_2$ showed a dose-dependent increase in ROS levels. The EC$_{50}$ value for ROS following treatment with 100 μM H$_2$O$_2$ was 80.33 μM. (h) The wound healing experiment revealed that the relative healing area of the CoCl$_2$ experimental group (4 h, 9 h, and 12 h of CoCl$_2$ treatment) was less than that of the control group. (ns, not significant; *p < 0.05, scale bar is 500 μm).

45

3.1.3 Selection of Conditioned Medium for Different Experiments

To monitor the influence of stem cells on ECs, we searched for the appropriate concentrations of the stem cell-conditioned medium. First, we observed the cell morphology of the HUVECs in complete medium, serum-free medium，and a medium containing 5% FBS. Morphological analysis revealed that in the absence of serum, ECs underwent apoptosis after 24h (Figure 6a). Next, we added the supernatant of ASCs to ECs at different concentrations and observed the morphology and viability of ECs. We also observed their cell status with and without serum. ECs showed better growth and survival in the presence of serum. Moreover, the addition of 40% to 60% of ASC supernatant did not affect the cell survival (Figure 6b). To ensure the integrity of the experiment, we mixed the whole medium with different concentrations of ASC supernatant and simultaneously observed the cell morphology and viability. The most suitable experimental condition was a mixture of whole medium and 50% of ASC supernatant (Figure 6c). We also studied the effect of cell culture media on co-culture. First, we mixed the media with different concentrations to observe the morphology of ECs and ASCs. (Figure 6d). Results showed that the mixture of 50% was the most suitable medium concentration for stable survival and growth of cells. Next, the co-culture was subjected to $CoCl_2$ to better understand the interaction between hypoxia and stem cells. The results of the MTT assay showed that after 4 h of $CoCl_2$ treatment, ASCs favored the cell viability of HUVECs (Figure 6e).
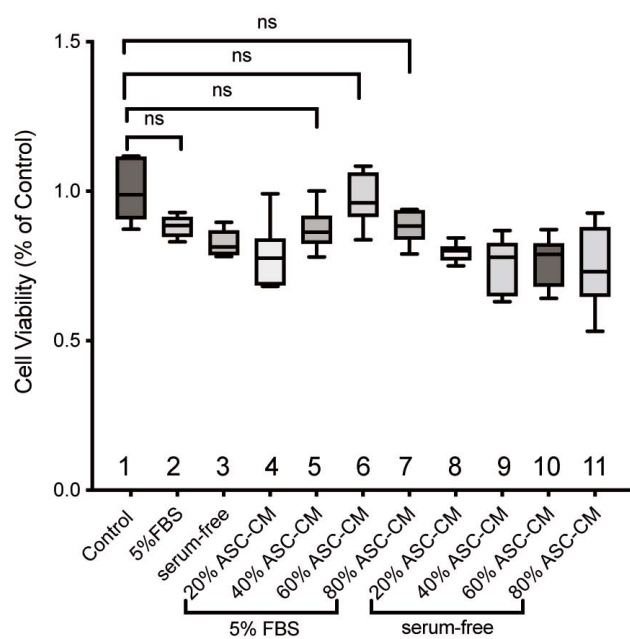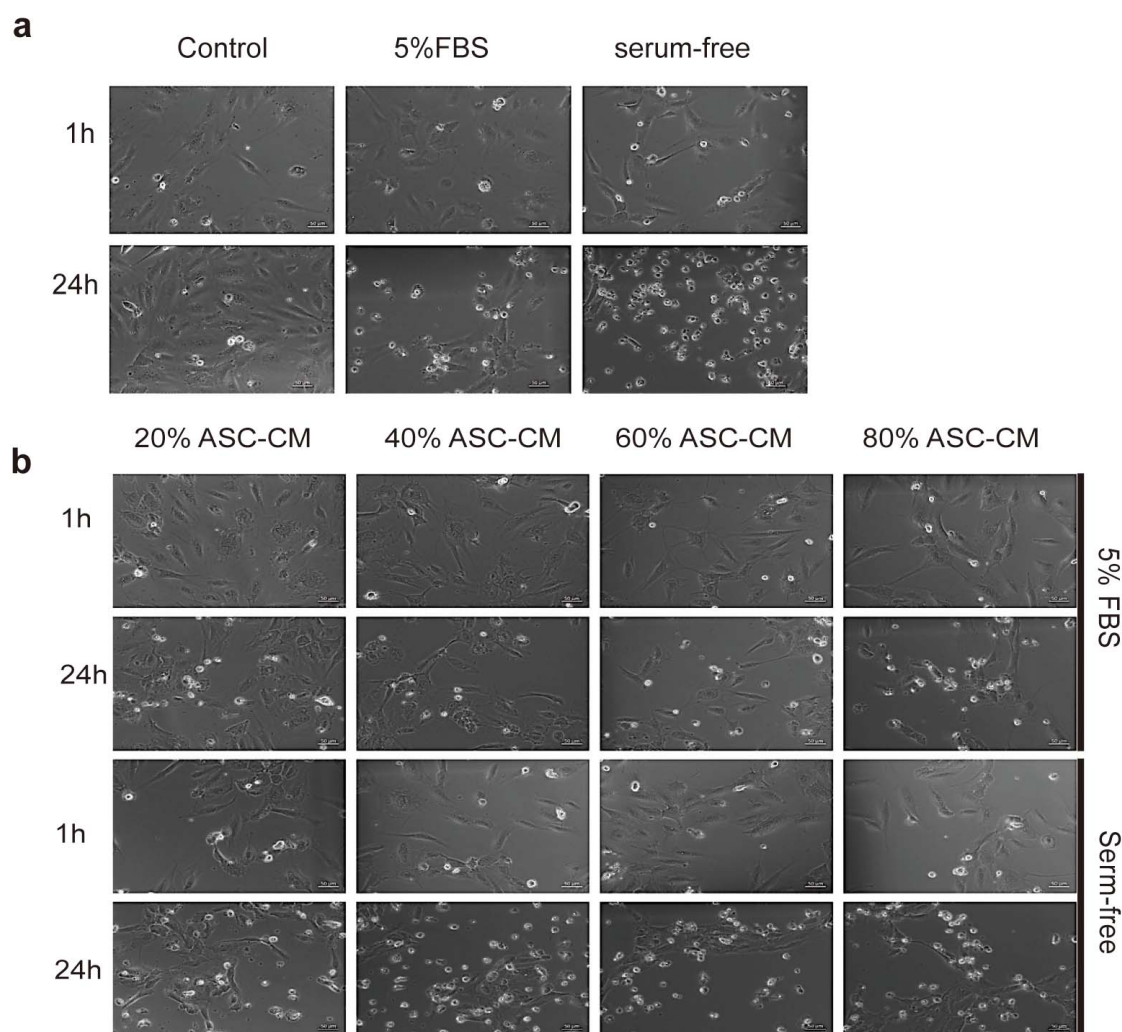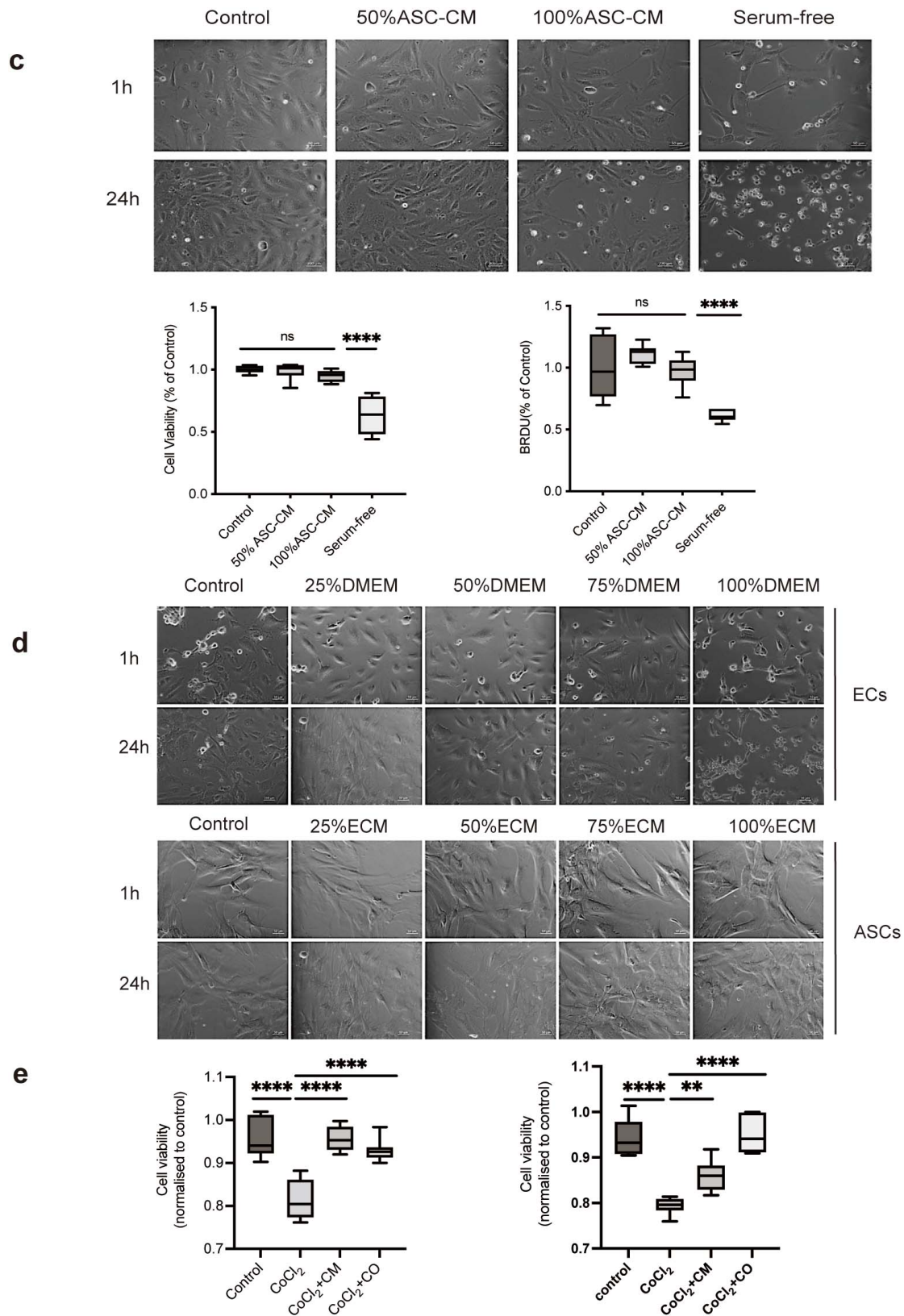
Figure 6 Selection of culture medium for co-culture condition. (a) The morphology of HUVECs in serum-containing and serum-free media was observed (scale bar is 100 μm). **(b)** The morphology of HUVECs in ASC-conditioned medium with and without serum (20%, 40%, 60%, 80%) was observed. The cell viability assay revealed no significant difference between the 60%

ASC-conditioned medium and the control group (scale bar is 100 μm). **(c)** Cell morphology of HUVECs in ASC-conditioned medium with serum-free, 50% and 100% serum are shown (scale bar is 100 μm). **(d)** Cell morphology of endothelial cells in DMEM medium, cell morphology of adipose stem cells in endothelial cell culture medium (scale bar is 100 μm). **(e)** In MTT assays, HUVEC cell viability in the mixture of adipose stem cells and cobalt chloride is not significantly different from the controls. The cell viability assay revealed no significant difference between the 50% ASC-conditioned medium and the control group. (ns, not significant; ** $p < 0.001$, **** $p < 0.00001$).

3.1.4 Angiogenic Function

For angiogenesis, HUVECs require an intact migratory ability and the cells should be viable. Moreover, the balance between ROS generation and absorption is a crucial factor. MTT analysis revealed that $CoCl_2$ significantly reduced the cell viability of HUVECs, and ASC-CM and ASC-CO reversed this effect (Figure7 c). Moreover, the results of the scratch assay confirmed this finding. $CoCl_2$ reduced the migration rate as compared to controls. This effect was reversed following treatment with ASCs (Figure7 a). With respect to tube formation, HUVECs showed the ability to form connections and grids under cell culture conditions (Figure7 b). $CoCl_2$ treatment significantly reduced the number of grids and connection points. ASC-CM and ASC-CO significantly increased the number of meshes and junctions under $CoCl_2$ treatment. We also simultaneously monitored the dynamic changes in ROS levels (Figure7 d). The ROS levels increased significantly following treatment with $CoCl_2$; however, treatment with ASCs reversed this effect. In conclusion, the results of cell viability, migration, and tube formation assay indicated that $CoCl_2$ interfered

with the angiogenic function in HUVECs, which was recovered by ASC treatment.
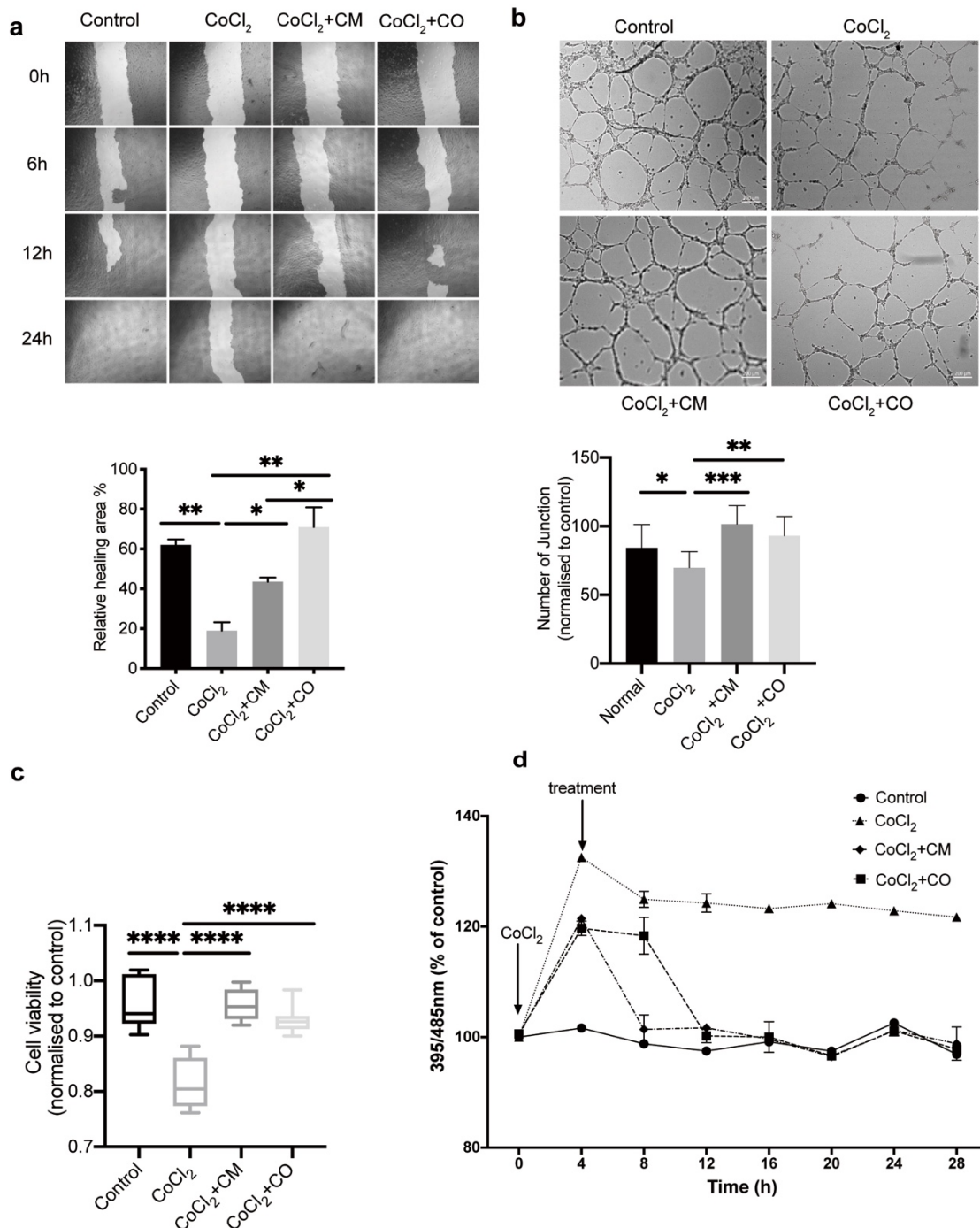
Figure 7 The angiogenic function of the adipose stem cells under different conditions (a) The scratch assay results showed that CoCl$_2$ significantly decreased the migration rate of HUVECs. The ASC-CM and ASC-CO significantly increased the migration rate following CoCl$_2$ treatment (scale bar is 500 μm). **(b)** The tube formation assay results showed that the number of meshes, and junctions significantly reduced with CoCl$_2$ treatment. ASC-CM and ASC-CO significantly

increased the number of meshes and junctions under CoCl$_2$ treatment (scale bar is 200 μm). **(c)** The MTT assay results indicated that CoCl$_2$ significantly decreased the viability of HUVECs. ASC-CM and ASC-CO significantly reversed this effect. **(d)** Treatment with CoCl$_2$ for 4 h significantly increased the ROS levels. The effect was reversed by ASC-CM and ASC-CO therapy for 24 h, and the therapeutic effects of ASC-CM were exerted earlier than ASC-CO. (*p < 0.05, ** p < 0.001, *** p < 0.0001, **** p < 0.00001)

3.1.5 Dynamic Changes in ER Ca^{2+} and Cytoplasmic Ca^{2+}

The impairment of the angiogenic function may indicate that the ER Ca^{2+} recovery ability could reduce hypoxia. This may explain the salvage of the angiogenic function observed after incubation with ASCs. To confirm this hypothesis, we investigated how Calcium homeostasis was influenced by CoCl$_2$ of ASCs.

HUVECs transduced with D1ER were stained with an ER-tracker red. Results showed that D1ER was only expressed in the ER. SP5 confocal microscopy using different channels revealed that both YFP and CFP from D1ER were expressed throughout the cells. To determine the function of D1ER, photobleaching was performed in 10 regions of interest (ROIs). Results indicated that the mean FRET efficiency was about 20%, which was in line with that reported in a previous study[96]. This confirmed functionality of our Calcium sensor.

In addition, different reagents were successfully used to increase and decrease the ER Ca^{2+}, as reflected by the FRET ratio. These results (Table 10) demonstrated that the D1ER worked well in reflecting dynamic changes in ER Ca^{2+} (Figure 8).

51
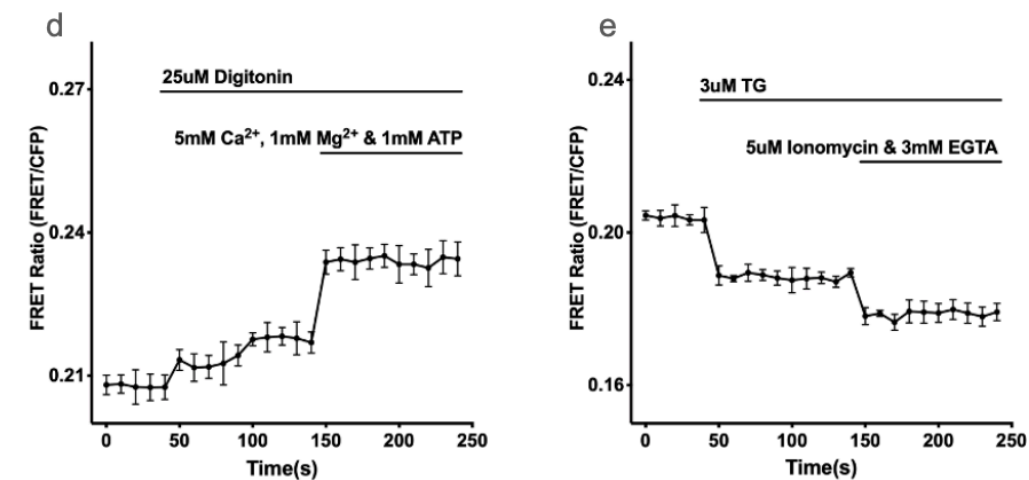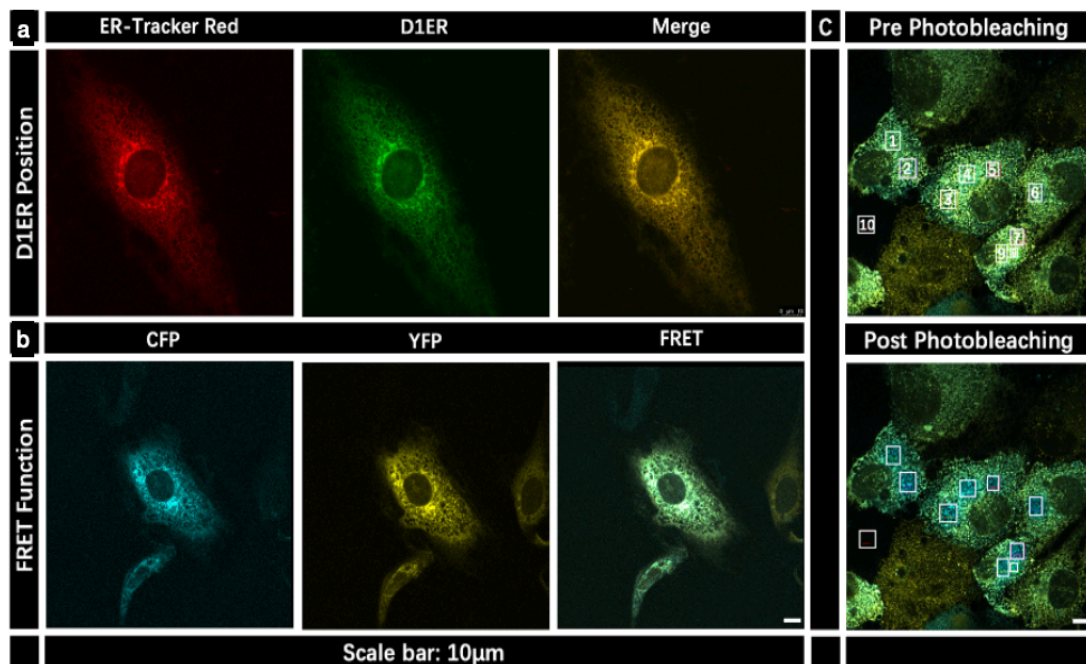
Figure 8 Testing functionality of D1ER sensor. (a) HUVECs transduced with D1ER were stained with ER-Tracker red. D1ER is only expressed in the ER. **(b)** Using the SP5 confocal microscopic system we confirmed that cells were able to express both YFP and CFP. **(c)** 10 ROIs were randomly chosen to estimate FRET efficiency. After photobleaching, the mean FRET efficiency was 20.24% (**Table 10**). **(d)** Different reagents were used to increase and decrease ER Ca2+, which were reflected by the FRET ratio. FRET ratio increased under the treatment of Digitonin, and medium containing Ca^{2+}, Mg^{2+}, and ATP. **(e)** FRET ratio decreased under the therapy of TG, ionomycin, and EGTA.

Table 10 Measurement of FRET Efficiency (%)

	CFP Pre Photobleaching	CFP Post Photobleaching	YFP Pre Photobleaching	YFP Post Photobleaching	FRET Efficiency
ROI1	70.42	84.44	63.6	1.75	17.04%
ROI 2	79.45	97.73	77.88	1.84	18.70%
ROI3	87.6	108.24	103.96	2.18	19.07%
ROI4	95.78	119.54	117.85	2.35	19.88%
ROI5	75.7	99.17	118.9	2.23	23.67%
ROI6	84.73	109.85	123.45	2.42	22.86%
ROI7	67.2	83.15	87.03	1.75	19.18%
ROI8	70.22	87.37	79.23	2.12	19.62%
ROI9	101.73	130.7	138.94	2.88	22.16%
ROI10	5.34	5.4	2.45	2.03	1.04%

ROI: region of interest

After 4 h of treatment with $CoCl_2$, the FRET ratio decreased significantly. This effect was reversed by ASC-CM and ASC-CO treatment for 24 h; the effect of ASC-CM was exerted earlier than ASC-CO (Figure 9a). Results of SP5 microscopy revealed that HUVECs treated with $CoCl_2$ displayed a significantly lower FRET ratio than control cells. In addition, the ASC-CM and ASC-CO treatment significantly increased the FRET ratio in the $CoCl_2$ group and reached normal levels (Figure 9b). These findings were considered important since depletion of ER Ca^{2+} stores resulted in ER stress and activated the UPR. Non-resolved ER stress can cumulatively cause cell death.

For confirmation, we also used the ratiometric fluorescent dye Fura-2. Fura-2 binds to free intracellular calcium. After 4 h of treatment with $CoCl_2$, the Fura-2 ratio increased significantly as compared to controls. Incubation by ACSs decreased the ratio over 24 h. ASC-CM exerted the effect earlier than ASC-CO. In summary, we found hypoxia to perturb the Calcium homeostasis within the cytoplasm and the ER (Figure 9c). We further investigated whether this also impaired endoplasmic reticulum stress.
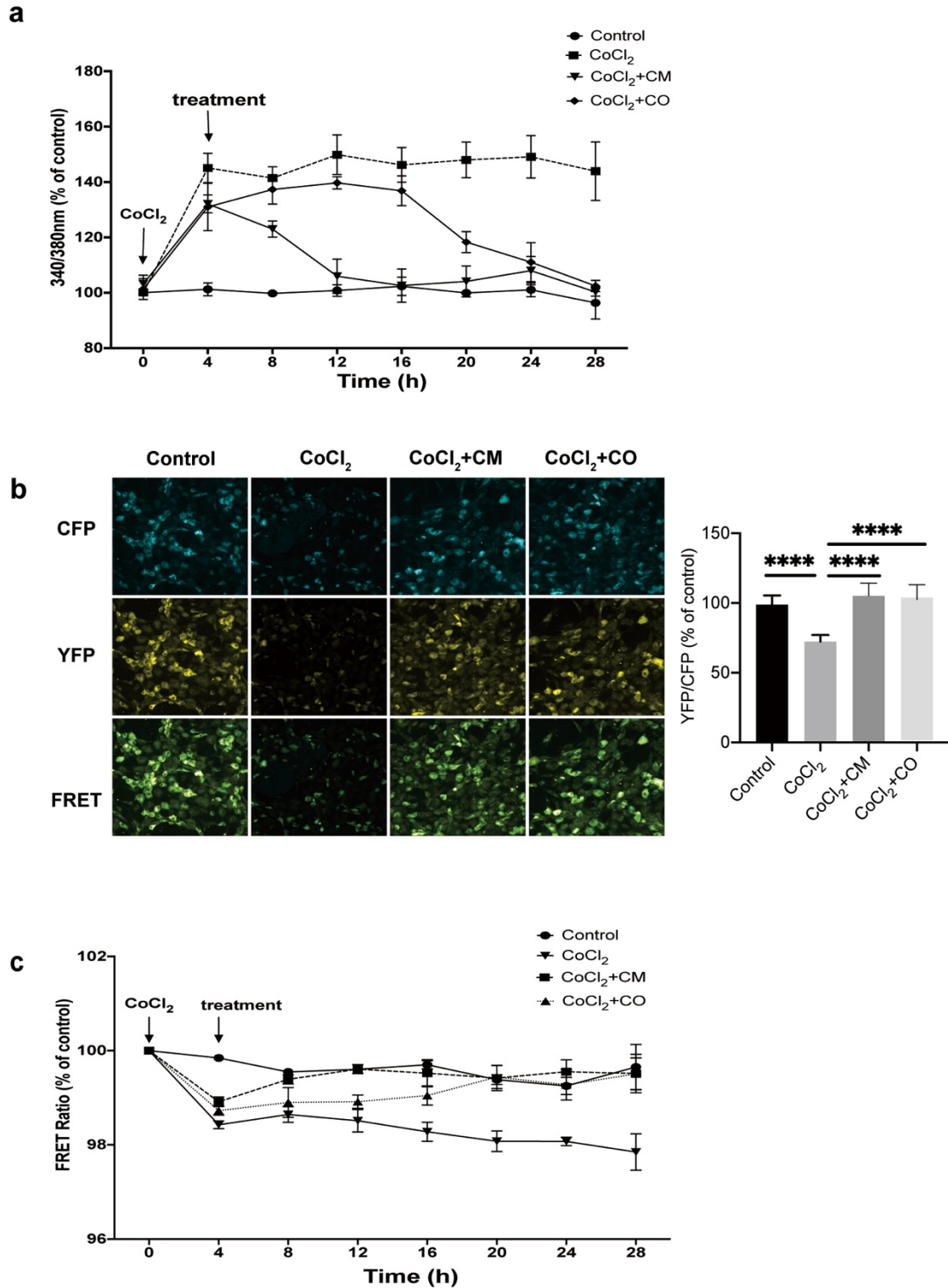
Figure 9 Hypoxia and calcium ion dynamic change (a) Treatment with CoCl2 for 4 h significantly increased the Fura-2 ratio. This effect was reversed by ASC-CM and ASC-CO treatment for 24 h. The therapeutic effect of ASC-CM was exerted earlier than ASC-CO. **(b)** HUVECs treated with CoCl2 displayed a significantly lower FRET ratio than control cells. The ASC-CM and ASC-CO treatments significantly increased the FRET ratio in CoCl2 groups and reached a normal level (scale bar is 75 μm). **(c)** Treatment with CoCl2 significantly decreased the FRET ratio.

This effect was reversed by ASC-CM and ASC-CO treatment in 24 h. The therapeutic effect of ASC-CM was exerted earlier than ASC-CO. (**** $p < 0.00001$).

3.1.6 Western Blotting on ER Stress *in vitro*

The results of western blots supplement the results of the dynamic changes of calcium ions in cells. The results of the dynamic changes of calcium ions indicate that hypoxia indeed leads to ER stress. 4 hours $CoCl_2$ treatment, led to high expression of BIP, ATF6 and XBP1 in HUVECs, with the stem cell treatment (co-culture, conditioned medium), the expression of these factors was reduced，but the expression level is still higher than the control group. $CoCl_2$ treatment did not influence CHOP expression, it also remained largely unchanged under the treatment of tunicamycin. This experiment shows that stem cells may ameliorate the damage caused by hypoxia in endothelial cells. At the same time, it shows that the concentration of cobalt chloride we used did not lead to cell apoptosis, Tunicamycin (TUN) 2.0µg/ml was used to induce UPR in HUVECs.

(Figure 10).
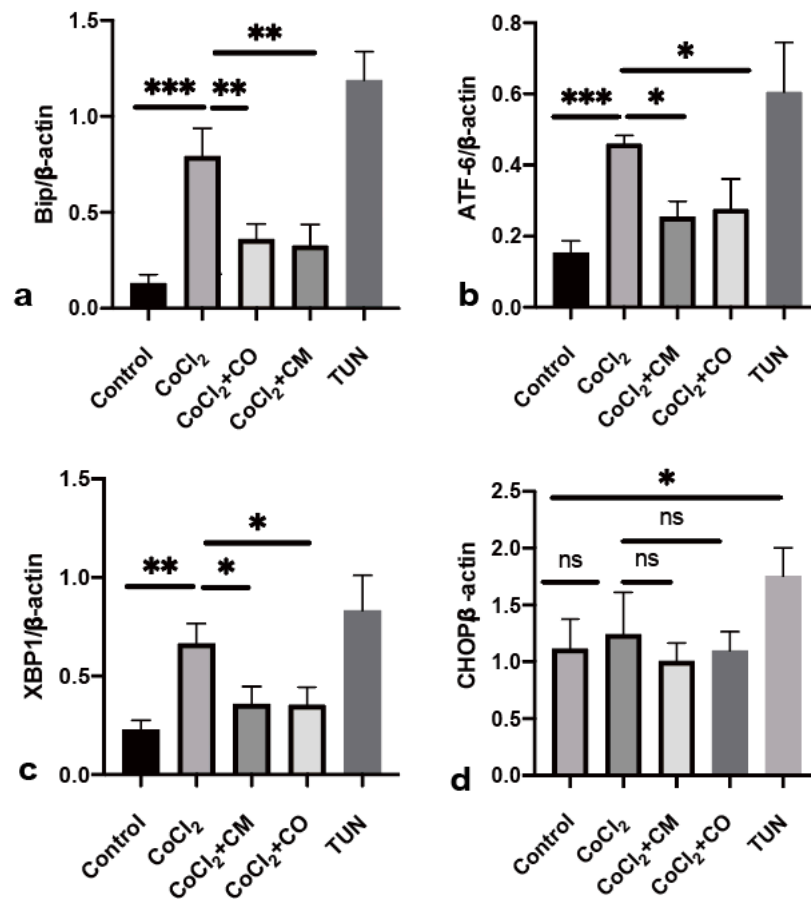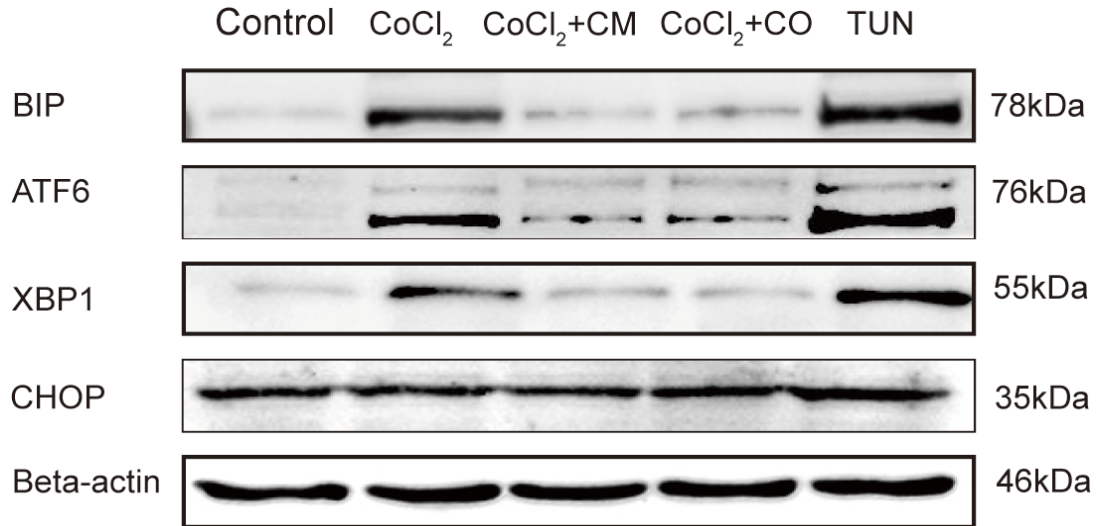
Figure 10 UPR western blotting *in vitro.* **(a)** ASC-CO and ASC-CM reduced the expression of BIP, incubations with tunicamycin (TUN) 2.0µg/ml, and CoCl₂. **(b)** ASC-CO and ASC-CM reduced the protein expression of ATF6, incubations with tunicamycin, and CoCl₂. **(c)** The protein expression of CHOP and tunicamycin was high. Differences were not present in other groups. **(d)** ASC-CO and ASC-CM reduced the protein expression of XBP1, incubations with tunicamycin, and CoCl₂. (ns, not significant; *p < 0.05, ** p < 0.001, *** p < 0.0001).

3.2 Results From *in vivo* Experiments

3.2.1   APOE$^{-/-}$ Mice and PAD Model

Atherosclerosis-prone apolipoprotein E-deficient (APOE$^{-/-}$) mice display poor lipoprotein clearance with a subsequent accumulation of cholesterol ester-enriched particles in the blood, which promote the development of atherosclerotic plaques[54]. Double ligature of the right femoral artery was performed on 24 mice successfully to induce hindlimb ischemia to model PAD. The procedure was successfully performed in the control group (12 mice) and treatment group (12 mice) （Figure 11）
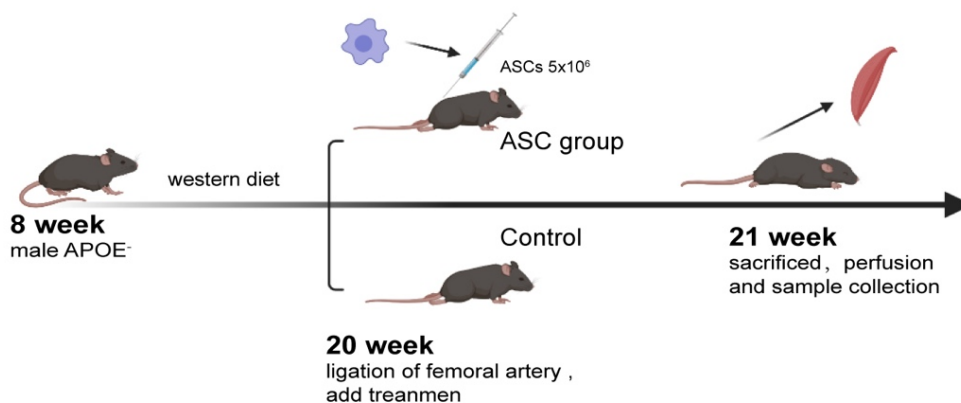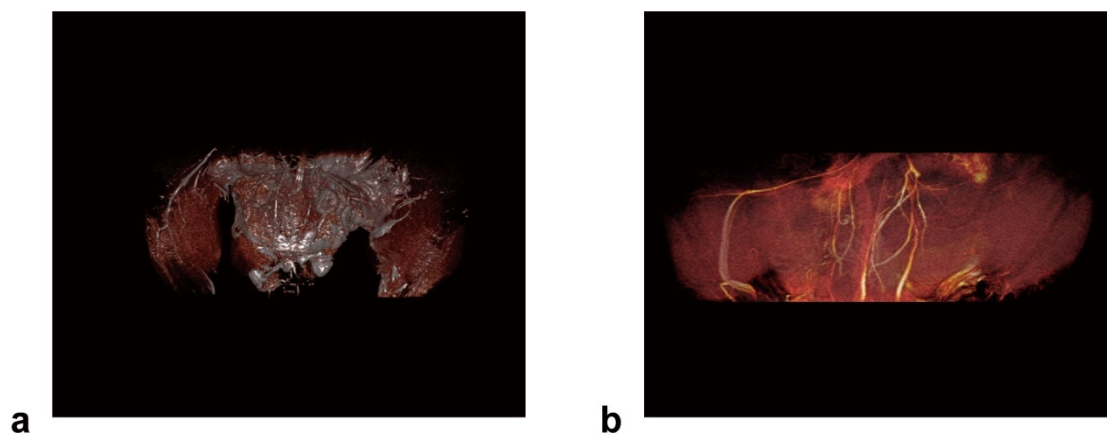

**Figure 11. PAD timeline model in APOE$^{-/-}$ mice.**

Magnetic resonance imaging (MRI) scans indicated that the proximal and distal regions of the right FA showed no perfusion, confirming the successful establishment of the model (Figure 12).

Figure 12. A representative MRI and 3D reconstruction of an operated mice. The **(a)** MRI scan and **(b)** 3D reconstruction results showed that the arterial blood flow of the right lower extremity had been effectively cut off.

After DLFA, the control group was treated with saline, whereas the treatment group was administered 100µl ASCs (1×10^8 cells/ml) injection, injected into 5 different muscle localizations of the right hindlimb (20µl each localization). Two mice in the control group died after the procedure (Figure 13 a). To study changes in the body weight, mice were weighed before the DLFA procedure (pre-DLFA) and 7 days after the DLFA surgery (post-DLFA). Mice showed significantly less weight loss after injection of ASCs (Figure 13 b).
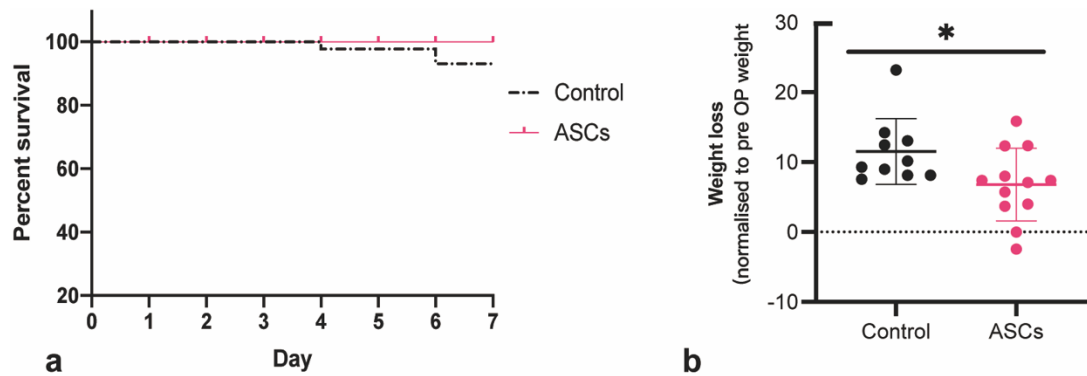
Figure 13 ASC treated APOE$^{-/-}$ mice loose significantly less weight in comparison to control after CLI. (a) The survival curve results showed that two mice in the control group died after the surgery, whereas no mice in the treatment group died after the surgery. **(b)** Compared with the control group, the treatment group exhibited smaller differences in weight before and after the surgery. (*p < 0.05).

### 3.2.2 Histological Analysis in APOE$^{-/-}$ Mice Muscle Specimens

The H&E staining of the right GM myofibers exhibited irregular areas of ischemic necrosis. Proliferating satellite cells replaced the necrotic myofibers and were distributed in a mass and with irregular dispersion. Myofibers were infiltrated with inflammatory multinucleated macrophages, with extremely few regenerated myofibers. The transverse sections of these regenerated myofibers were round, the cytoplasm was stained red, and one small or multiple nuclei were located at the center (Figure 14 a). Treatment with ASCs effectively reduced these signs of muscle inflammation and necrosis of the right lower limb.

The ELISA assay revealed that the stem cell treatment group significantly reduced the expression of LDH in muscle tissue (Figure 14 b, left). However, Mb in the GM was relatively increased after treatment with ASCs (Figure 14 b right). With IHC , used Anti-CD31 antibody staining was performed to identify ECs of the vessel in the GM samples. ImageJ was used to evaluate the CD31-

positive areas, a surrogate for microvascular density, in each of the five fields of view (×40) for each sample. Ischemic hindlimbs exhibited significantly more microvascular density than the non-ischemic side following treatment with ASCs (Figure 14 c). Analysis of H&E sections of the thoracoabdominal aorta showed no significant difference in plaque load in $APOE^{-/-}$ mice between the treatment and control groups (Figure 14 d).

The serum tests revealed no significant difference in the levels of cholesterol (Figure 14 e, left), CK (Figure 14 e, middle), and triglycerides (Figure 14 e, right) between the two groups of mice. Finally, no significant difference was observed in the general condition of mice before and after the surgery.
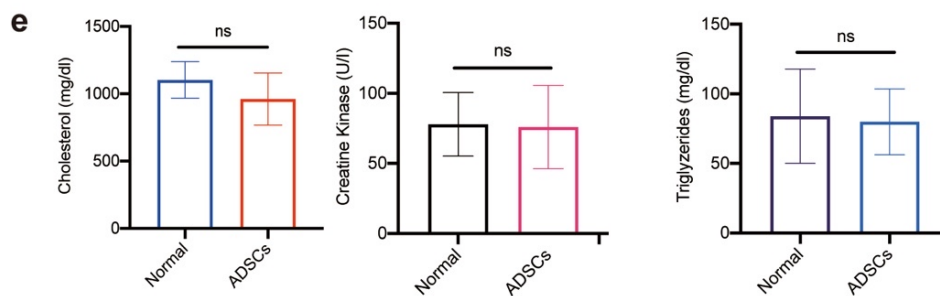
In summary, after the surgery, the ASC stem cell treatment effectively improved PAD-induced ischemic tissue necrosis, reduced inflammation, and effectively increased the microvascular density in the muscle specimens (biceps femoris, Gastrocnemius，Rectus femoris).

d

D1

e
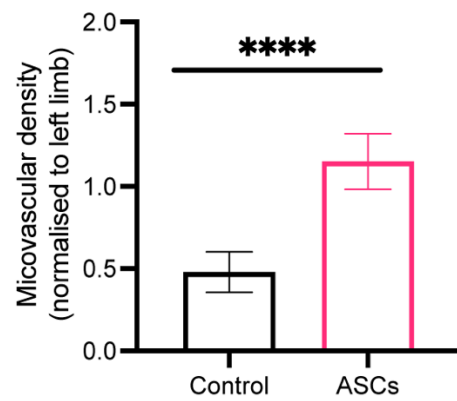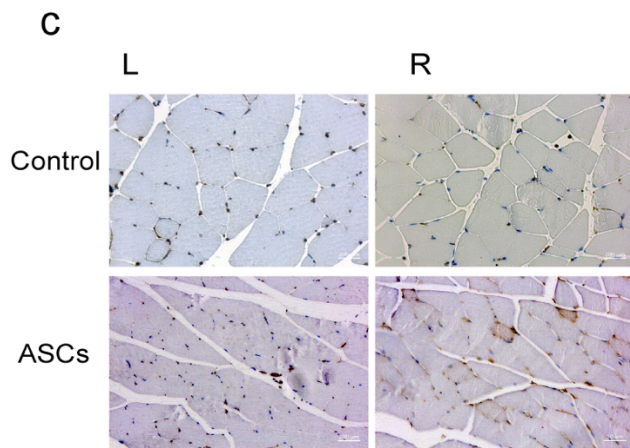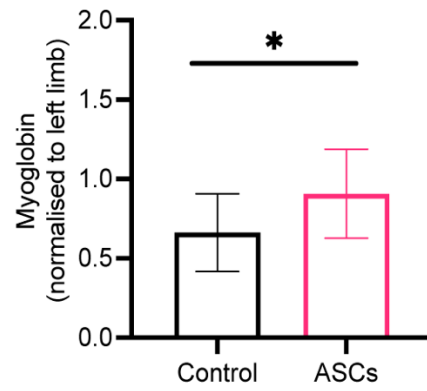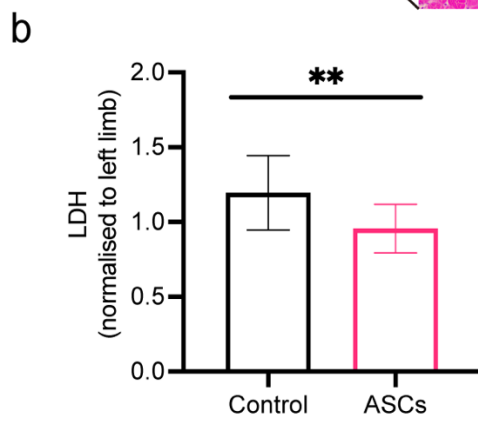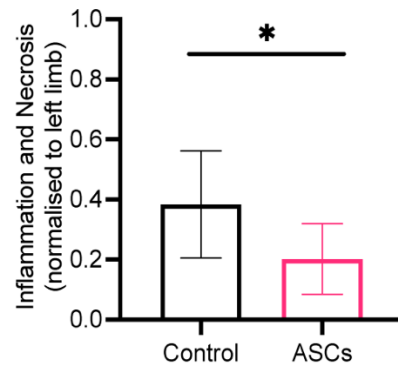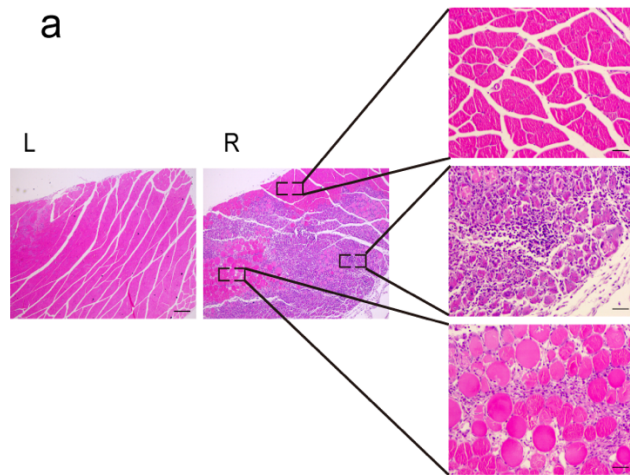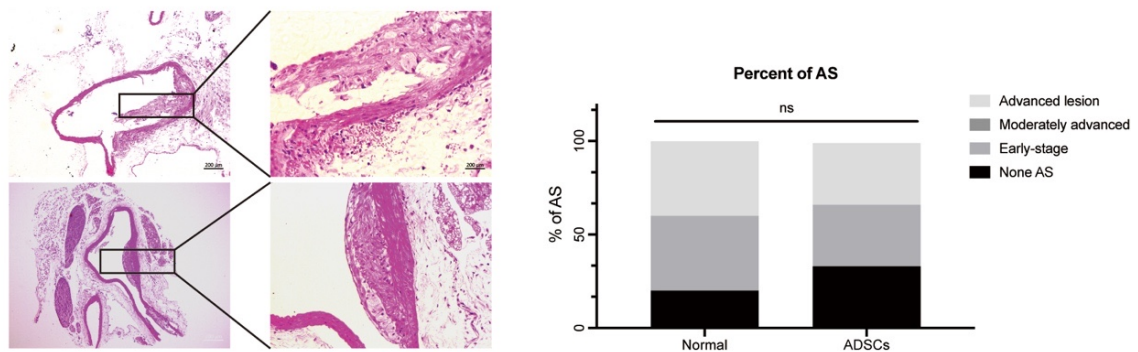
Figure 14 ASCs treatment protects the Gastronemius muscle against hypoxia induced injury. (a)
H&E staining of the right gastrocnemius. After ASC treatment, the proliferating satellite cells
replaced the necrotic muscle fibers and were distributed in large numbers and as irregularly
dispersed forms. Muscle fibers showed inflammatory infiltration of multinucleated macrophages.
The cross-section of these regenerated muscle fibers appeared round; the cytoplasm was
stained red, multiple nuclei in the center. Stem cells effectively reduced the inflammation and
necrosis in muscle tissue (scale bar is 200 μm and 100μm). **(b)** The LDH assay revealed that
stem cell treatment significantly reduced LDH in muscle tissue. Myoglobin in the GM was
relatively increased after ASC treatment. **(c)** Immunohistochemical staining revealed that CD31
staining of paraffin-embedded sections showed that the microcapillary density in the stem cell
treatment group was higher than that in the control group (scale bar is 200 μm). **(d)** H&E
sections of the thoracoabdominal aorta. No significant difference was observed between the
treatment and the control groups (scale bar is 200 μm and 50μm). **(e)** A comparison of serum
levels of CK (left), cholesterol (middle), and triglycerides (right) revealed no significant
difference between the two groups of mice. (ns, not significant, *p < 0.05, ** p < 0.001, **** p <
0.00001).

3.2.3 Hind Limb Ischemia and ER Stress

WB was performed to measure expression levels of BIP, ATF6, XBP1 and CHOP in protein isolated from muscle specimens. First, left and right (treated) hindlimbs of the mice were compared within the treatment group and the control group. The expression levels of BIP, ATF6, XBP1 and CHOP were lower in the treatment group than in the control group. Especially differences in ATF6 were highly significant (Figure 15). This data shows that after treatment with adipose stem cells, stem cells can indirectly or directly alleviate damage caused by ischemia and hypoxia.
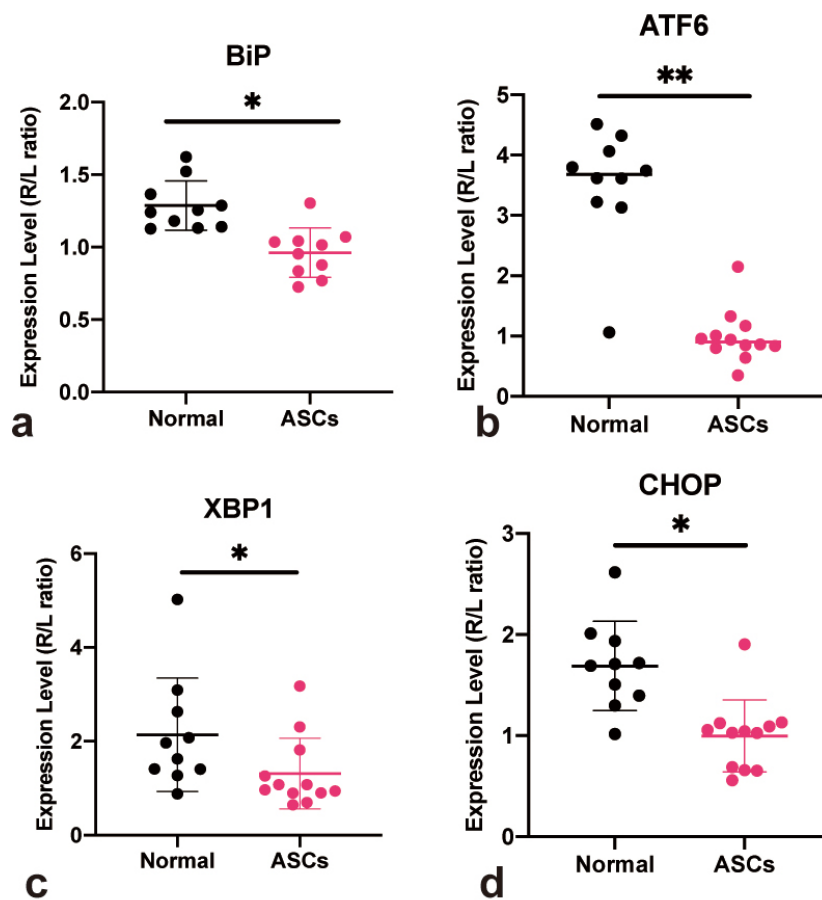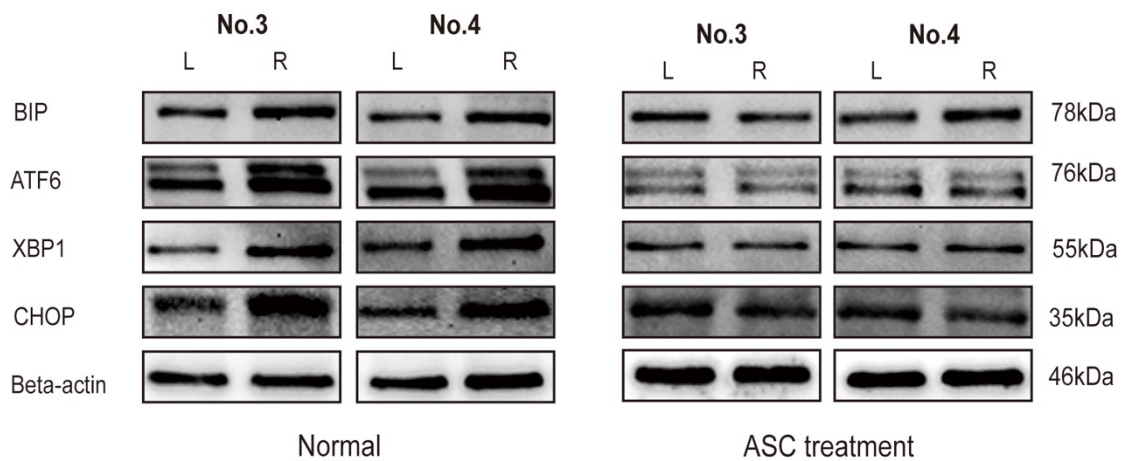
Figure 15 UPR WB *in vivo* **(a)** A comparison of protein expression of BIP revealed a significant difference between the treatment and control groups. **(b)** A comparison of the expression of protein ATF6 revealed a significant difference between the treatment and control groups. **(c)** A comparison of the protein expression of XBP1 revealed a significant difference between the treatment and control groups. **(d)** A comparison of the expression of protein CHOP revealed a significant difference between the treatment and control groups. (*p < 0.05, ** p < 0.001).

4 DISCUSSION

We evaluated the effects of ASCs on EC functions under hypoxia both *in vitro* and *in vivo*. PAD is caused by AS of the peripheral blood vessels and results in ischemia. Tissue hypoxia can cause partial dysfunction of vascular cells, manifested as alterations in EC migration, proliferation, and neovascularization. Stem cell therapy has emerged as an alternative treatment modality for PAD. In this regard, ASCs are the most favorable stem cells because of several beneficial properties including the ability to differentiate into several cell lineages, anti-apoptotic activity, the ability to secrete bioactive soluble factors, anti-inflammatory effect, and anti-bacterial effect. Furthermore, ASCs improve vascularization in injured tissues by inducing the expression of angiogenic cytokines. For instance, VEGF secreted by ASCs improves tissue vascularity by stimulating ECs to promote angiogenesis and growth. We explored the therapeutic mechanism of ASCs *in vivo* using a mouse PAD model and investigated the effects of ASC therapy by injecting ASCs into the lower limb muscles of ApoE$^{-/-}$ mice (n=12). Furthermore, we investigated the effects of ASCs on ECs using a series of *in vitro* experiments.

4.1 Establishing an *in vitro* Environment Mimicking Hypoxia

We established an *in vitro* hypoxic environment that reflected the levels of cellular, biochemical, and molecular hypoxia responses. Although the best hypoxia model is the one induced by true hypoxia, many laboratories lack a

66

hypoxia chamber. Not all kinds of experiments can be performed using carbon dioxide incubators because oxygen will re-enter the chamber at each opening. Moreover, this process is expensive. Therefore, frequently a chemically induced hypoxia model is used. A commonly used chemical to induce hypoxia is $CoCl_2$, which strongly stabilizes HIF-1α and HIF-2α under normoxic conditions for several hours in a dose- and time-dependent manner. HIF-1α/2α stabilization was observed after 2 h, with a maximum effect at 12 to 48 h and with a $CoCl_2$ concentration between 100 and 300 μM. The exact $CoCl_2$ concentration will depend on the susceptibility or resistance of the kind of cells used. For example, Horev-Azaria determined the cell viability in Caco-2, MDCK, HepG2, A459, and NCIH441 cells lines treated with 0 to 1.0 mM $CoCl_2$ for 48 and 72 h and observed a completely different behavior and susceptibility to $CoCl_2$ concentrations and incubation times for each cell line[116]. The reported $CoCl_2$ IC_{50} values for IMR-32, PC-3, and A548 cell lines were 30.3, 92.1, and 125.3 μM, respectively, at 24 h, which were lower than those observed for non-cancerous 293T cells [86].

We have also used $CoCl_2$ to simulate an *in vitro* hypoxic environment. The WB results indicated that the expression of HIF-1α increased with increasing concentration of $CoCl_2$. The EC_{50} value of $CoCl_2$ was 29.72 μM. We observed that $CoCl_2$ treatment ≥ 4h significantly increased HIF-1α expression. We used PI and Annexin V staining and flow cytometry to detect $CoCl_2$-induced cell death in ECs and observed that after 4 h of treatment, HUVECs did not undergo

extensive apoptosis. Treatment with different concentrations of $CoCl_2$ revealed a concentration-dependent increase in ROS levels. Results showed that 80.33 μM $CoCl_2$ reached half the effect of inducing ROS. Furthermore, hypoxia reduced the migration rate of HUVECs. These data demonstrate that HUVECs treated with 80 µM $CoCl_2$ for 4 h established a hypoxia cell model. Therefore, we selected 80 to 100 µM $CoCl_2$ as a suitable concentration range and selected 4 h of $CoCl_2$ as a treatment time that did not induce extensive apoptosis of ECs.

4.2 Do Stem Cells Promote Angiogenesis in Endothelial Cells ?

Our primary aim was to establish an *in vitro* pathological model of PAD to explore the therapeutic mechanism of stem cells. Vessel occlusion in PAD is attributed to the formation of atherosclerotic plaques. Atherosclerosis initiates with the deposition of fatty streaks on the vessel wall, damaging the vascular endothelium and triggering an inflammatory response[42]. Plaques partially block the blood vessels and obstruct the blood flow, resulting in tissue ischemia and hypoxia. The therapeutic effect of ASCs is attributed to tissue repair and regeneration, ability to differentiate into several cell lineages, and ability to migrate (homing) to injured tissues. Other treatment mechanisms include angiogenesis, anti-apoptotic activity, and the ability to secrete bioactive soluble factors. Of these, angiogenesis under hypoxia may be relevant for developing an efficient PAD therapy. ASCs contribute to angiogenesis both directly and indirectly through supporting cells and paracrine activity. ROS control vascular

cell migration and proliferation, and its homeostasis ensures normal angiogenesis. To better observe the paracrine effects of stem cells, we designed two experimental conditions: adding a stem cell-conditioned medium and co-culturing of ECs and stem cells. Using *ex vivo* and *in vivo* experiments, Kim et al. first demonstrated that ASCs accelerated wound healing[83,84]. Furthermore, they observed that the conditioned media of ASC (ASC-CM), obtained from primary cultured fibroblasts, stimulated the migration of dermal fibroblasts to the wounded area[84]. In addition, ASCs secrete a variety of growth factors such as basic fibroblast growth factor (bFGF), keratinocyte growth factor (KGF), transforming growth factor (TGF-β).

Several experiments were conducted to obtain a suitable conditioned medium and stable co-culture conditions. The experimental results showed that mixing the whole medium with 50% ASC supernatant produced the most suitable experimental condition. This minimized the effect of growth factors on FBS. In addition, 50% was the most suitable medium concentration (50% DMEM + 50% advance endothelial medium) for the survival and growth of cells.

The MTT analysis revealed that $CoCl_2$ significantly reduced the cell viability of HUVECs, whereas ASC-CM and ASC-CO reversed this effect, indicating that ASCs promoted the survival of ECs under hypoxia. Migration assays revealed that $CoCl_2$ reduced the migration rate. Surprisingly, ASCs indirectly or directly accelerated the migration rate of ECs in the ASC-CO group. Results of the endothelial tube formation assay showed that the number of meshes, and

junctions was significantly reduced following CoCl$_2$ treatment. The effect was significantly reversed by ASC-CM and ASC-CO following CoCl$_2$ treatment. CoCl$_2$ simultaneously increased the levels of ROS; this effect was reversed by ASC-CM and ASC-CO therapy in 24 h. Furthermore, the therapeutic effect of ASC-CM was exerted earlier than ASC-CO. ASC conditioned medium produced delayed effects, which could be attributed to the time taken by ASCs to exert a paracrine effect on ECs in the co-culture.

Thus, ASCs accelerated the migration ability, tube formation ability, and viability of ECs under hypoxia through paracrine signaling. In contrast, ASCs reduced the production of ROS under hypoxia, indicating that they promoted the angiogenesis ability of ECs.

4.3 Effect of Stem Cells on Calcium Ions in Endothelial Cells

Our results showed that ASCs directly or indirectly promoted the survival and angiogenic functions of ECs under hypoxia. ER, a ubiquitous organelle, is responsible for synthesis, proper folding, maturation, and assembly of proteins before these are further processed by the Golgi apparatus. Stable ER Ca^{2+} concentration or homeostasis is crucial to maintain the cellular functions. ER Ca^{2+} depletion causes misfolding or unfolding of proteins, resulting in their accumulation within the ER lumen. This in turn causes ER stress and activates the UPR[47,48]. UPR is a normal adaptive and protective mechanism to reduce the rate of protein synthesis, increase the folding ability of proteins, and help misfolded or unfolded proteins to enter cellular degradation pathways[85].

Nevertheless, non-resolved ER stress can cumulatively cause cell death[86,87]. Mungai et al. and Gusarova et al. demonstrated the existence of this pathway under hypoxia in osteosarcoma cells and alveolar epithelial cells[87-89].

Hypoxia reduces the ER Ca^{2+} restoring ability by increasing the release of ER Ca^{2+}. In parallel, an influx of extracellular Ca^{2+} is induced, consequently increasing the cytoplasmic Ca^{2+} concentrations[89,90]. The overloading of cytoplasmic Ca^{2+} subsequently induces cell dysfunction and apoptosis, indicating prolonged or severe hypoxia[91-93]. The imbalance in the interaction between cytoplasmic Ca^{2+} and ER Ca^{2+} is a sign of ER stress, which affects the survival of the endothelium.

We used functional microscopy to analyze the FRET ratio. After 4 h of $CoCl_2$ treatment, the FRET ratio significantly reduced, reflecting a decrease in ER Ca^{2+} under hypoxia. ASC-CM and ASC-CO treatment for 24 h reversed this effect, with the therapeutic effect of ASC-CM occurring earlier than that of ASC-CO. The results of FRET microscopy showed that the FRET ratio of HUVECs treated with $CoCl_2$ was significantly lower than that of control cells.

Dynamic changes in cytoplasmic Ca^{2+} were detected by fluorescence using Fura-2AM. Compared with the control group, the Fura-2 ratio of the $CoCl_2$ group increased significantly after 4 h of $CoCl_2$ treatment due to $CoCl_2$-induced elevation in cytoplasmic Ca^{2+}. However, the therapeutic effect of ASCs reduced the ratio in the following 24 h although the impact from ASC-CM was displayed earlier than ASC-CO. These results implied that $CoCl_2$ mimicking a hypoxic

71

pathological condition of ECs, results in a continuous decrease in ER Ca^{2+} and increase in cytoplasmic Ca^{2+} due to reduced ER Ca^{2+} restoring ability. This could result in dysfunctional neovessels. The ASC-conditioned medium and adipose co-culture group reversed the above calcium imbalance under the same conditions. These results also indicated that stem cells regulate ER stress.

4.4 Stem Cells under Hypoxia induce survival in Endothelial Cells

Hypoxic stress induces global gene expression changes by altering the cell's metabolic and angiogenic pathways and restoring oxygen homeostasis, thereby promoting cell survival[95-97]. A failure of these repair and adaptive mechanisms causes cells to modify their gene expression profiles and induce programmed cell death[97-107]. However, these changes are accompanied by deregulation of mitochondrial and ER functions, reflected by perturbations in protein folding and trafficking[109]. Erratic protein folding activates another specific stress response pathway, the UPR promotes cellular survival by restoring endoplasmic and mitochondrial homeostasis via distinct signaling networks[109,110]. Although not completely understood, delineating the mutual crosstalk and response pathways between these stresses is essential to establish new therapeutic interventions for cardiovascular diseases. Critical changes in mitochondrial functions occur during hypoxia causing elevated ROS levels. Furthermore, the proper folding of mitochondria-encoded, as well as the import and corresponding refolding of mitochondrial nucleus-encoded proteins,

is crucial for the proper functioning of this organelle. Hence, prolonged hypoxia eventually results in perturbations in mitochondrial protein folding and activation of a related specific stress response mechanism known as the mitochondrial UPR[110,111]. Although ECs are the primary effectors of the adaptive cellular response to hypoxia, the majority of current research on this signaling pathway involves cancer cells[115-118].

BiP initiates the UPR by dissociating three proteins, namely PERK, IRE1α, and ATF6, from the ER lumen. Our *in vitro* and *in vivo* results revealed that all ER stress sensors (BIP, ATF6, CHOP, and XBP1) are activated once tunicamycin is processed. However, only BIP, ATF6, and XBP1 are activated under virtual hypoxia. We observed that the expression of these proteins was reduced in the stem cell treatment group. Stem cells effectively alleviated endothelial dysfunction under hypoxic conditions by strengthening ATF6 and initiating a transcriptional program to restore ER homeostasis; inducing BIP expression; promoting protein chaperones and lipid synthesis; stimulating ER degradation, and enhancing N-glycosylation of XBP1 by increasing the ER's folding capacity, as well as increasing the expression of chaperones and proteins involved in ER-associated degradation (by ER degradation-enhancing α-mannosidase-like protein [EDEM]) and vesicular trafficking. The inactivation of CHOP could be attributed to the fact that the $CoCl_2$ concentration used was insufficient to activate it, leading to cell death.

4.5 Therapeutic Effects of ASCs in the ApoE$^{-/-}$ PAD Mouse Model

ApoE$^{-/-}$ mice can be used to study abnormal fat metabolism and hyperlipidemia symptoms, such as total cholesterol, triglycerides, very low-density lipoproteins, and medium-density lipoproteins, which mimic clinically relevant PAD. H&E staining of the aorta confirmed the establishment of AS, following alimentation with Western diet[114].

We demonstrated *in vivo* in ApoE$^{-/-}$ PAD mice model that the ASC treatment improved the functional recovery within 7 days after surgery. On the seventh day, the weight loss of the ASC group was better than that of the control group, with a statistically significant difference. This validated the therapeutic effect of ASCs. To further confirm this finding, we performed IHC staining to assess MVD (Microvascular density) in the hindlimb GM. Because capillaries supply the nutrients (oxygen, glucose, etc.) and dispose cellular waste products, MVD is a crucial prognostic factor for PAD [24]. Patients with PAD and poor prognosis usually show low MVD[112, 113]. In the ApoE$^{-/-}$ PAD mice model, the MVD ratio of the ASC group was significantly higher than that of the control group, indicating that ASC treatment enhanced angiogenesis, which was also observed in our *in vitro* experiments. ASC therapy-induced neovascularization is conducive for restoring metabolic homeostasis, thereby improving functional recovery. In addition, the average LDH levels in the muscles in the ASC group were lower than those in the control group; moreover, these results were statistically significant, indicating that ASCs could improve metabolic homeostasis.

Our comprehensive *in vivo* and *in vitro* experiment results explained the ability of ASCs to improve the angiogenesis of ECs, possibly by enhancing the recovery ability of ER Ca^{2+} under hypoxic conditions. Although we detected dynamic changes in ER Ca^{2+} and cytoplasmic Ca^{2+} in HUVECs *in vitro*, we could not these in the fresh tissues of the hindlimbs of mice, especially in the ECs of the tissues. This weakens the integrity of our experimental results.

In vivo results reported tissue ischemia in the right lower limb of mice caused by surgery. We observed protein expression of BIP, CHOP, XBP1, and ATF6 following the treatment with ASCs. The protein expression, especially of ATF6, was reduced. Further studies will have to answer if the effect of ASCs can be attributed to ATF6. Compared with *in vitro* experiments, CHOP was activated in-vivo in mice due to surgery-induced ischemia and hypoxia.

4.6 Limitations

Our study had certain limitations. First, objective laboratory conditions and experimental time constraints did not allow us to use hypoxic chambers to simulate true hypoxia; we used $CoCl_2$ to mimic hypoxic conditions. Therefore, our results are potentially incomparable with those observed in a truly hypoxic environment. An *in vitro* hypoxic model could be established using a hypoxic chamber in the future to overcome this shortcoming.

Second, we did not explore the paracrine effects of stem cells, such as growth factors, and VEGF tracking on ECs. Third, to detect the relationship between ER Ca^{2+} recovery ability and EC angiogenesis function using D1ER and Fura-2 AM, we detected the dynamic changes in ER Ca^{2+} and cytoplasmic Ca^{2+} in HUVECs. However, we could not use these assays to detect these changes in the fresh tissues of the hindlimbs of mice, especially in the ECs of the tissues.

Fourthly, previous studies have reported immunomodulatory and anti-inflammatory effects of ASCs[16-18]. Unfortunately, we did not include relevant experiments, such as the detection of inflammatory factors, for example, IL-6, IL-1, and TNF. We only observed the inflammatory manifestations of ischemic hind limbs by H&E staining.

Finally, we performed WB in the GM sample, which includes not only ECs but also muscle cells, macrophages, fibroblasts, and other kinds of cells. Therefore, the results of *in vitro* experiments cannot fully explain the specific therapeutic effects of ASCs on ECs. These shortcomings did not enable us to directly

answer all questions about the underlying mechanism of therapeutic effects of ASCs on ECs. Thus, more studies are warranted in the future to explore the therapeutic mechanism of stem cells in more depth.

5 SUMMARY

Peripheral arterial disease (PAD) is a chronic circulatory disease, characterized by narrowed arteries and reduced blood flow to the extremities.

The beneficial effects of adipose stem cells (ASCs) have been exploited in several clinical trials as a therapeutic intervention for PAD[24,25]. To further explore the therapeutic mechanism of stem cells on PAD, we designed this study in ECs under hypoxia.

First, to mimic the pathological mechanism of PAD *in vitro*, we used $CoCl_2$ to create a hypoxic environment in the ECs. We found that the viability and migration of ECs were reduced under hypoxia. Next, we used a stem cell-conditioned medium to co-cultivate ECs and stem cells.

We investigated the angiogenic functions of ECs under hypoxia and studied the 24-h dynamic changes in calcium ions in the ER and the cytoplasm of ECs and used the SP5 microscopy platform to detect the intracellular FRET ratio. After $CoCl_2$ treatment, the FRET ratio significantly reduced, reflecting a decrease in ER Ca^{2+} under hypoxia. ASC-CM and ASC-CO treatment for 24 h reversed this effect, with the therapeutic effect of ASC-CM occurring earlier than that of ASC-CO

By western blotting the effects of stem cells on the UPR pathways were analyzed. *In vitro* and *in vivo* (using a hind limb ischemia model) revealed that all ER stress sensors (BIP, ATF6, CHOP, and XBP1) are activated once tunicamycin is processed. BIP, ATF6, and XBP1 are activated under virtual

hypoxia. Using the hind limb ischemia model, ASC were demonstrated to ameliorate the effect of ischemia on muscle tissue. Animals showed less muscle necrosis, less inflammation and lover levels of muscle enzymes after ASC injection.

Taken together, these data indicate that ASCs may represent an interesting treatment option for PAD patients with no conventional option of revascularization.

6 CONCLUSION

The findings of the study conclude the following:

1. $CoCl_2$ can be used to stimulate a hypoxic environment in ECs.

2. ASCs promoted angiogenesis in ECs, which was manifested as increased cell migration, enhanced tube formation, improved cell vitality, and balanced ROS levels.

3. ASCs promoted calcium ion balance in the cytoplasm and ER.

4. ASCs relieved ER stress in ECs under hypoxia.

5. Infusion of ASCs into $ApoE^{-/-}$ mice enhanced the intramuscular angiogenesis in ischemic lower limbs, reduced the inflammation, and decreased necrosis and apoptosis of cells in the muscle tissue.

7 REFERENCES

1. Semenza, GL: Hypoxia and human disease-and the Journal of Molecular Medicine. *J Mol Med (Berl),* 85**:** 1293-1294, 2007.
2. Lee, JW, Ko, J, Ju, C, Eltzschig, HK: Hypoxia signaling in human diseases and therapeutic targets. *Exp Mol Med,* 51**:** 1-13, 2019.
3. Nangaku, M, Eckardt, KU: Hypoxia and the HIF system in kidney disease. *J Mol Med (Berl),* 85**:** 1325-1330, 2007.
4. Tuder, RM, Yun, JH, Bhunia, A, Fijalkowska, I: Hypoxia and chronic lung disease. *J Mol Med (Berl),* 85**:** 1317-1324, 2007.
5. Semenza, GL: Vascular responses to hypoxia and ischemia. *Arterioscler Thromb Vasc Biol,* 30**:** 648-652, 2010.
6. Speer, R, Ratan, RR: Hypoxic Adaptation in the Nervous System: Promise for Novel Therapeutics for Acute and Chronic Neurodegeneration. *Adv Exp Med Biol,* 903**:** 221-243, 2016.
7. Brahimi-Horn, MC, Chiche, J, Pouyssegur, J: Hypoxia and cancer. *J Mol Med (Berl),* 85**:** 1301-1307, 2007.
8. Zinkernagel, AS, Johnson, RS, Nizet, V: Hypoxia inducible factor (HIF) function in innate immunity and infection. *J Mol Med (Berl),* 85**:** 1339-1346, 2007.
9. Kevil, CG, Bir, SC, Pattillo, CB, Akkus, NI: Peripheral Arterial Disease: Pathophysiology and Therapeutics. *Colloquium Series on Integrated Systems Physiology: From Molecule to Function,* pp1-82, 2013.
10. Kaschwich, M, Behrendt, CA, Heydecke, G, Bayer, A, Debus, ES, Seedorf, U, Aarabi, G: The Association of Periodontitis and Peripheral Arterial Occlusive Disease-A Systematic Review. *Int J Mol Sci,* 20, 2019.
11. Vos, T, Flaxman, AD, Naghavi, M, Lozano, R: Years lived with disability (YLDs) for 1160 sequelae of 289 diseases and injuries 1990-2010: a systematic analysis for the Global Burden of Disease Study 2010. *Lancet,* 380**:** 2163-2196, 2012.
12. Fowkes, FG, Rudan, D, Rudan, I: Comparison of global estimates of prevalence and risk factors for peripheral artery disease in 2000 and 2010: a systematic review and analysis. *Lancet,* 382**:** 1329-1340, 2013.
13. Norgren, L, Hiatt, WR, Dormandy, JA, Nehler, MR, Harris, KA, Fowkes, FG, Group, TIW: Inter-Society Consensus for the Management of Peripheral Arterial Disease (TASC II). *J Vasc Surg,* 45 Suppl S**:** S5-67, 2007.
14. Lawall, H, Huppert, P, Espinola-Klein, C, Rumenapf, G: The Diagnosis and Treatment of Peripheral Arterial Vascular Disease. *Dtsch Arztebl Int,* 113**:** 729-736, 2016.
15. Uccioli, L, Meloni, M, Izzo, V, Giurato, L, Merolla, S, Gandini, R: Critical limb ischemia: current challenges and future prospects. *Vasc Health Risk Manag,* 14**:** 63-74, 2018.

16. Murabito, JM, Evans, JC, Nieto, K, Larson, MG, Levy, D, Wilson, PW: Prevalence and clinical correlates of peripheral arterial disease in the Framingham Offspring Study. *Am Heart J,* 143**:** 961-965, 2002.

17. Adam, DJ, Beard, JD, Cleveland, T: Bypass versus angioplasty in severe ischaemia of the leg (BASIL): multicentre, randomised controlled trial. *Lancet,* 366**:** 1925-1934, 2005.

18. Stoyioglou, A, Jaff, MR: Medical treatment of peripheral arterial disease: a comprehensive review. *J Vasc Interv Radiol,* 15**:** 1197-1207, 2004.

19. Steg, PG, Bhatt, DL, Wilson, PW, D'Agostino, R, Sr.: One-year cardiovascular event rates in outpatients with atherothrombosis. *JAMA,* 297**:** 1197-1206, 2007.

20. Caro, J, Migliaccio-Walle, K, Ishak, KJ, Proskorovsky, I: The morbidity and mortality following a diagnosis of peripheral arterial disease: long-term follow-up of a large database. *BMC Cardiovasc Disord,* 5**:** 14, 2005.

21. Economic, UNDo, Affairs, S: *World Population Ageing 2019*, United Nations, 2020.

22. Abu Dabrh, AM, Steffen, MW, Undavalli, C: The natural history of untreated severe or critical limb ischemia. *J Vasc Surg,* 62**:** 1642-1651 e1643, 2015.

23. Aboyans, V, Ricco, JB, Bartelink, MEL, Bjorck, M: 2017 ESC Guidelines on the Diagnosis and Treatment of Peripheral Arterial Diseases. *Eur Heart J,* 39**:** 763-816, 2018.

24. Demaison, C, Parsley, K, Brouns, G, Scherr, M, Battmer, K, Kinnon, C, Grez, M, Thrasher, AJ: High-level transduction and gene expression in hematopoietic repopulating cells using a human immunodeficiency virus type 1-based lentiviral vector containing an internal spleen focus forming virus promoter. *Hum Gene Ther,* 13**:** 803-813, 2002.

25. Maier, P, Herskind, C, Fleckenstein, K, Spier, I: MDR1 gene transfer using a lentiviral SIN vector confers radioprotection to human CD34+ hematopoietic progenitor cells. *Radiat Res,* 169**:** 301-310, 2008.

26. Bjorck, M, Earnshaw, JJ, Acosta, S, Bastos Goncalves, F: Editor's Choice - European Society for Vascular Surgery (ESVS) 2020 Clinical Practice Guidelines on the Management of Acute Limb Ischaemia. *EJVES,* 59**:** 173-218, 2020.

27. Inampudi, C, Akintoye, E, Ando, T, Briasoulis, A: Angiogenesis in peripheral arterial disease. *Curr Opin Pharmacol,* 39**:** 60-67, 2018.

28. Melfi, R, Ricottini, E: Antiplatelet therapy for peripheral artery disease. *Cardiovasc Diagn Ther,* 8**:** 663-677, 2018.

29. Saeedi, P, Halabian, R, Imani Fooladi, AA: A revealing review of mesenchymal stem cells therapy, clinical perspectives and Modification strategies. *Stem Cell Investig,* 6**:** 34, 2019.

30. Pittenger, MF, Discher, DE, Peault, BM, Phinney, DG, Hare, JM, Caplan, AI: Mesenchymal stem cell perspective: cell biology to clinical progress. *NPJ Regen Med,* 4**:** 22, 2019.

31. Moazzami, K, Moazzami, B, Roohi, A, Nedjat, S, Dolmatova, E: Local intramuscular transplantation of autologous mononuclear cells for critical lower limb ischaemia. *Cochrane Database Syst Rev,12***:** CD008347, 2014.

32. Hu, C, Li, L: Preconditioning influences mesenchymal stem cell properties in vitro and in vivo. *J Cell Mol Med,* 22**:** 1428-1442, 2018.

33. Naji, A, Eitoku, M, Favier, B, Deschaseaux, F, Rouas-Freiss, N, Suganuma, N: Biological functions of mesenchymal stem cells and clinical implications. *Cell Mol Life Sci,* 76**:** 3323-3348, 2019.

34. Chu, DT, Nguyen Thi Phuong, T, Tien, NLB, Tran, DK: Adipose Tissue Stem Cells for Therapy: An Update on the Progress of Isolation, Culture, Storage, and Clinical Application. *J Clin Med,* 8, 2019.

35. Si, Z, Wang, X, Sun, C, Kang, Y, Xu, J, Wang, X, Hui, Y: Adipose-derived stem cells: Sources, potency, and implications for regenerative therapies. *Biomed Pharmacother,* 114**:** 108765, 2019.

36. Hassan, WU, Greiser, U, Wang, W: Role of adipose-derived stem cells in wound healing. *Wound Repair Regen,* 22**:** 313-325, 2014.

37. Shingyochi, Y, Orbay, H, Mizuno, H: Adipose-derived stem cells for wound repair and regeneration. *Expert Opin Biol Ther,* 15**:** 1285-1292, 2015.

38. Mazini, L, Rochette, L, Amine, M, Malka, G: Regenerative Capacity of Adipose Derived Stem Cells (ADSCs), Comparison with Mesenchymal Stem Cells (MSCs). *Int J Mol Sci,* 20, 2019.

39. Paino, F, La Noce, M, Di Nucci, D: Human adipose stem cell differentiation is highly affected by cancer cells both in vitro and in vivo: implication for autologous fat grafting. *Cell Death Dis,* 8**:** e2568, 2017.

40. Aykan, A, Ozturk, S, Sahin, I, Avcu, F, Sagkan, RI, Isik, S: The Effects of Hydrogen Sulfide on Adipocyte Viability in Human Adipocyte and Adipocyte-Derived Mesenchymal Stem Cell Cultures Under Ischemic Conditions. *Ann Plast Surg,* 75**:** 657-665, 2015.

41. Elshaer, SL, Evans, W, Pentecost, M, Lenin, R: Adipose stem cells and their paracrine factors are therapeutic for early retinal complications of diabetes in the Ins2(Akita) mouse. *Stem Cell Res Ther,* 9**:** 322, 2018.

42. Gadelkarim, M, Abushouk, AI, Ghanem, E, Hamaad, AM, Saad, AM, Abdel-Daim, MM: Adipose-derived stem cells: Effectiveness and advances in delivery in diabetic wound healing. *Biomed Pharmacother,* 107**:** 625-633, 2018.

43. Ribatti, D: Judah Folkman, a pioneer in the study of angiogenesis. *Angiogenesis,* 11**:** 3-10, 2008.

44. Cao, SS, Kaufman, RJ: Endoplasmic reticulum stress and oxidative stress in cell fate decision and human disease. *Antioxid Redox Signal,* 21**:** 396-413, 2014.

45. Paik, JY, Jung, KH, Lee, JH, Park, JW, Lee, KH: Reactive oxygen species-driven HIF1alpha triggers accelerated glycolysis in endothelial cells exposed to low oxygen tension. *Nucl Med Biol,* 45**:** 8-14, 2017.

46. Forrester, SJ, Kikuchi, DS, Hernandes, MS, Xu, Q, Griendling, KK: Reactive Oxygen Species in Metabolic and Inflammatory Signaling. *Circ Res,* 122**:** 877-902, 2018.

47. Minamino, T, Komuro, I, Kitakaze, M: Endoplasmic reticulum stress as a therapeutic target in cardiovascular disease. *Circ Res,* 107**:** 1071-1082, 2010.

48. Malhotra, JD, Miao, H, Zhang, K, Wolfson, A, Pennathur, S, Pipe, SW, Kaufman, RJ: Antioxidants reduce endoplasmic reticulum stress and improve protein secretion. *Proc Natl Acad Sci U S A,* 105**:** 18525-18530, 2008.

49. Panday, A, Sahoo, MK, Osorio, D, Batra, S: NADPH oxidases: an overview from structure to innate immunity-associated pathologies. *Cell Mol Immunol,* 12**:** 5-23, 2015.

50. Tavender, TJ, Springate, JJ, Bulleid, NJ: Recycling of peroxiredoxin IV provides a novel pathway for disulphide formation in the endoplasmic reticulum. *EMBO J,* 29**:** 4185-4197, 2010.

51. Bedard, K, Krause, KH: The NOX family of ROS-generating NADPH oxidases: physiology and pathophysiology. *Physiol Rev,* 87**:** 245-313, 2007.

52. Brandes, RP, Weissmann, N, Schroder, K: NADPH oxidases in cardiovascular disease. *Free Radic Biol Med,* 49**:** 687-706, 2010.

53. Park, WJ, Oh, JG: SERCA2a: a prime target for modulation of cardiac contractility during heart failure. *BMB Rep,* 46**:** 237-243, 2013.

54. Lo Sasso, G, Schlage, WK, Boue, S, Veljkovic, E, Peitsch, MC, Hoeng, J: The Apoe(-/-) mouse model: a suitable model to study cardiovascular and respiratory diseases in the context of cigarette smoke exposure and harm reduction. *J Transl Med,* 14**:** 146, 2016.

55. Aley, PK, Porter, KE, Boyle, JP, Kemp, PJ, Peers, C: Hypoxic modulation of Ca2+ signaling in human venous endothelial cells. Multiple roles for reactive oxygen species. *J Biol Chem,* 280**:** 13349-13354, 2005.

56. Evangelista, AM, Thompson, MD, Weisbrod, RM, Pimental, DR: Redox regulation of SERCA2 is required for vascular endothelial growth factor-induced signaling and endothelial cell migration. *Antioxid Redox Signal,* 17**:** 1099-1108, 2012.

57. Keeley, TP, Siow, RCM, Jacob, R, Mann, GE: Reduced SERCA activity underlies dysregulation of Ca(2+) homeostasis under atmospheric O2 levels. *FASEB J,* 32**:** 2531-2538, 2018.

58. Dooley, CT, Dore, TM, Hanson, GT, Jackson, WC, Remington, SJ, Tsien, RY: Imaging dynamic redox changes in mammalian cells with green fluorescent protein indicators. *J Biol Chem,* 279**:** 22284-22293, 2004.

59. Bers, DM: Cardiac sarcoplasmic reticulum calcium leak: basis and roles in cardiac dysfunction. *Annu Rev Physiol,* 76**:** 107-127, 2014.

60. Suresh, K, Servinsky, L, Jiang, H, Bigham, Z: Reactive oxygen species induced Ca(2+) influx via TRPV4 and microvascular endothelial

dysfunction in the SU5416/hypoxia model of pulmonary arterial hypertension. *Am J Physiol Lung Cell Mol Physiol,* 314**:** L893-L907, 2018.

61. Pati, S, Khakoo, AY, Zhao, J, Jimenez, F: Human mesenchymal stem cells inhibit vascular permeability by modulating vascular endothelial cadherin/beta-catenin signaling. *Stem Cells Dev,* 20**:** 89-101, 2011.

62. Baudin, B, Bruneel, A, Bosselut, N, Vaubourdolle, M: A protocol for isolation and culture of human umbilical vein endothelial cells. *Nat Protoc,* 2**:** 481-485, 2007.

63. Soleimani, M, Nadri, S: A protocol for isolation and culture of mesenchymal stem cells from mouse bone marrow. *Nat Protoc,* 4**:** 102-106, 2009.

64. Liu, MM, Flanagan, TC, Lu, CC, French, AT, Argyle, DJ, Corcoran, BM: Culture and characterisation of canine mitral valve interstitial and endothelial cells. *Vet J,* 204**:** 32-39, 2015.

65. Heydarkhan-Hagvall, S, Helenius, G, Johansson, BR, Li, JY, Mattsson, E, Risberg, B: Co-culture of endothelial cells and smooth muscle cells affects gene expression of angiogenic factors. *J Cell Biochem,* 89**:** 1250-1259, 2003.

66. Goers, L, Freemont, P, Polizzi, KM: Co-culture systems and technologies: taking synthetic biology to the next level. *J R Soc Interface,* 11, 2014.

67. Weiss, WM, Mulet-Sierra, A, Kunze, M, Jomha, NM, Adesida, AB: Coculture of meniscus cells and mesenchymal stem cells in simulated microgravity. *NPJ Microgravity,* 3**:** 28, 2017.

68. Bahmani, L, Taha, MF, Javeri, A: Coculture with embryonic stem cells improves neural differentiation of adipose tissue-derived stem cells. *Neuroscience,* 272**:** 229-239, 2014.

69. Azhdari Tafti, Z, Mahmoodi, M, Hajizadeh, MR, Ezzatizadeh, V, Baharvand, H, Vosough, M, Piryaei, A: Conditioned Media Derived from Human Adipose Tissue Mesenchymal Stromal Cells Improves Primary Hepatocyte Maintenance. *Cell J,* 20**:** 377-387, 2018.

70. Gimbrone, MA, Jr., Cotran, RS, Folkman, J: Human vascular endothelial cells in culture. Growth and DNA synthesis. *J Cell Biol,* 60**:** 673-684, 1974.

71. Lennikov, A, Mirabelli, P, Mukwaya, A, Schaupper, M: Selective IKK2 inhibitor IMD0354 disrupts NF-kappaB signaling to suppress corneal inflammation and angiogenesis. *Angiogenesis,* 21**:** 267-285, 2018.

72. Heiss, M, Hellstrom, M, Kalen, M: Endothelial cell spheroids as a versatile tool to study angiogenesis in vitro. *FASEB J,* 29**:** 3076-3084, 2015.

73. Hanson, GT, Aggeler, R, Oglesbee, D: Investigating mitochondrial redox potential with redox-sensitive green fluorescent protein indicators. *J Biol Chem,* 279**:** 13044-13053, 2004.

74. Albrecht, M, Henke, J, Tacke, S, Markert, M, Guth, B: Effects of isoflurane, ketamine-xylazine and a combination of medetomidine, midazolam and

fentanyl on physiological variables continuously measured by telemetry in Wistar rats. *BMC Vet Res,* 10**:** 198, 2014.

75. Niiyama, H, Huang, NF, Rollins, MD, Cooke, JP: Murine model of hindlimb ischemia. *J Vis Exp*, 2009.

76. Yu, J, Dardik, A: A Murine Model of Hind Limb Ischemia to Study Angiogenesis and Arteriogenesis. *Methods Mol Biol,* 1717**:** 135-143, 2018.

77. Del Giudice, C, Ifergan, G, Goudot, G: Evaluation of a new model of hind limb ischemia in rabbits. *J Vasc Surg,* 68**:** 849-857, 2018.

78. Appelhoff, RJ, Tian, YM, Raval, RR, Turley, H, Harris, AL, Pugh, CW, Ratcliffe, PJ, Gleadle, JM: Differential function of the prolyl hydroxylases PHD1, PHD2, and PHD3 in the regulation of hypoxia-inducible factor. *J Biol Chem,* 279**:** 38458-38465, 2004.

79. Fu, JD, Yao, JJ, Wang, H, Cui, WG, Leng, J, Ding, LY, Fan, KY: Effects of EGCG on proliferation and apoptosis of gastric cancer SGC7901 cells via down-regulation of HIF-1alpha and VEGF under a hypoxic state. *Eur Rev Med Pharmacol Sci,* 23**:** 155-161, 2019.

80. Abdel-Rahman Mohamed, A, M, MMM, Khalil, SR, Salem, GA, Ali, HA: Moringa oleifera extract attenuates the CoCl2 induced hypoxia of rat's brain: Expression pattern of HIF-1alpha, NF-kB, MAO and EPO. *Biomed Pharmacother,* 109**:** 1688-1697, 2019.

81. Munoz-Sanchez, J, Chanez-Cardenas, ME: The use of cobalt chloride as a chemical hypoxia model. *J Appl Toxicol,* 39**:** 556-570, 2019.

82. Zimmerman, MA, Biggers, CD, Li, PA: Rapamycin treatment increases hippocampal cell viability in an mTOR-independent manner during exposure to hypoxia mimetic, cobalt chloride. *BMC Neurosci,* 19**:** 82, 2018.

83. Zhou, BR, Xu, Y, Guo, SL, Xu, Y: The effect of conditioned media of adipose-derived stem cells on wound healing after ablative fractional carbon dioxide laser resurfacing. *Biomed Res Int,* 2013**:** 519126, 2013.

84. Kim, WS, Park, BS, Sung, JH, Yang, JM, Park, SB, Kwak, SJ, Park, JS: Wound healing effect of adipose-derived stem cells: a critical role of secretory factors on human dermal fibroblasts. *J Dermatol Sci,* 48**:** 15-24, 2007.

85. Tsang, KY, Chan, D, Bateman, JF, Cheah, KS: In vivo cellular adaptation to ER stress: survival strategies with double-edged consequences. *J Cell Sci,* 123**:** 2145-2154, 2010.

86. Sano, R, Reed, JC: ER stress-induced cell death mechanisms. *Biochim Biophys Acta,* 1833**:** 3460-3470, 2013.

87. Hetz, C, Papa, FR: The Unfolded Protein Response and Cell Fate Control. *Mol Cell,* 69**:** 169-181, 2018.

88. Gusarova, GA, Trejo, HE, Dada, LA, Briva, A: Hypoxia leads to Na,K-ATPase downregulation via Ca(2+) release-activated Ca(2+) channels and AMPK activation. *Mol Cell Biol,* 31**:** 3546-3556, 2011.

89. Arnould, T, Michiels, C, Alexandre, I, Remacle, J: Effect of hypoxia upon intracellular calcium concentration of human endothelial cells. *J Cell Physiol,* 152**:** 215-221, 1992.

90. Desireddi, JR, Farrow, KN, Marks, JD, Waypa, GB, Schumacker, PT: Hypoxia increases ROS signaling and cytosolic Ca(2+) in pulmonary artery smooth muscle cells of mouse lungs slices. *Antioxid Redox Signal,* 12**:** 595-602, 2010.

91. Zeng, B, Liao, X, Liu, L, Ruan, H, Zhang, C: Thyroid Hormone Diminishes Ca2+ Overload Induced by Hypoxia/Reoxygenation in Cardiomyocytes by Inhibiting Late Sodium Current and Reverse-Na+/Ca2+ Exchange Current. *Pharmacology,* 105**:** 63-72, 2020.

92. Bartoszewska, S, Collawn, JF: Unfolded protein response (UPR) integrated signaling networks determine cell fate during hypoxia. *Cell Mol Biol Lett,* 25**:** 18, 2020.

93. Diaz-Bulnes, P, Saiz, ML, Lopez-Larrea, C, Rodriguez, RM: Crosstalk Between Hypoxia and ER Stress Response: A Key Regulator of Macrophage Polarization. *Front Immunol,* 10**:** 2951, 2019.

94. Chen, J, Chen, J, Cheng, Y: Mesenchymal stem cell-derived exosomes protect beta cells against hypoxia-induced apoptosis via miR-21 by alleviating ER stress and inhibiting p38 MAPK phosphorylation. *Stem Cell Res Ther,* 11**:** 97, 2020.

95. Yang, Z, Zhao, TZ, Zou, YJ, Zhang, JH, Feng, H: Hypoxia Induces autophagic cell death through hypoxia-inducible factor 1alpha in microglia. *PLoS One,* 9**:** e96509, 2014.

96. Dunwoodie, SL: The role of hypoxia in development of the Mammalian embryo. *Dev Cell,* 17**:** 755-773, 2009.

97. Sendoel, A, Hengartner, MO: Apoptotic cell death under hypoxia. *Physiology (Bethesda),* 29**:** 168-176, 2014.

98. Strzyz, P: Cancer biology: Hypoxia as an off switch for gene expression. *Nat Rev Mol Cell Biol,* 17**:** 610, 2016.

99. Thiele, RH: Subcellular Energetics and Metabolism: A Cross-Species Framework. *Anesth Analg,* 124**:** 1857-1871, 2017.

100. Bargiela, D, Burr, SP, Chinnery, PF: Mitochondria and Hypoxia: Metabolic Crosstalk in Cell-Fate Decisions. *Trends Endocrinol Metab,* 29**:** 249-259, 2018.

101. Mazure, NM, Pouyssegur, J: Hypoxia-induced autophagy: cell death or cell survival? *Curr Opin Cell Biol,* 22**:** 177-180, 2010.

102. Bartoszewski, R, Moszynska, A, Serocki, M, Cabaj, A: Primary endothelial cell-specific regulation of hypoxia-inducible factor (HIF)-1 and HIF-2 and their target gene expression profiles during hypoxia. *FASEB J,* 33**:** 7929-7941, 2019.

103. Lenihan, CR, Taylor, CT: The impact of hypoxia on cell death pathways. *Biochem Soc Trans,* 41**:** 657-663, 2013.

104. Rosenbaum, DM, Michaelson, M, Batter, DK, Doshi, P, Kessler, JA: Evidence for hypoxia-induced, programmed cell death of cultured neurons. *Ann Neurol,* 36**:** 864-870, 1994.

105. Krock, BL, Skuli, N, Simon, MC: Hypoxia-induced angiogenesis: good and evil. *Genes Cancer,* 2**:** 1117-1133, 2011.

106. Bensellam, M, Maxwell, EL, Chan, JY, Luzuriaga, J, West, PK, Jonas, JC, Gunton, JE, Laybutt, DR: Hypoxia reduces ER-to-Golgi protein trafficking and increases cell death by inhibiting the adaptive unfolded protein response in mouse beta cells. *Diabetologia,* 59**:** 1492-1502, 2016.

107. Bartoszewski, R, Kroliczewski, J, Piotrowski, A, Jasiecka, AJ: Codon bias and the folding dynamics of the cystic fibrosis transmembrane conductance regulator. *Cell Mol Biol Lett,* 21**:** 23, 2016.

108. Wouters, BG, Koritzinsky, M: Hypoxia signalling through mTOR and the unfolded protein response in cancer. *Nat Rev Cancer,* 8**:** 851-864, 2008.

109. Bartoszewski, R, Rab, A, Fu, L, Bartoszewska, S, Collawn, J, Bebok, Z: CFTR expression regulation by the unfolded protein response. *Methods Enzymol,* 491**:** 3-24, 2011.

110. Maamoun, H, Benameur, T, Pintus, G, Munusamy, S, Agouni, A: Crosstalk Between Oxidative Stress and Endoplasmic Reticulum (ER) Stress in Endothelial Dysfunction and Aberrant Angiogenesis Associated With Diabetes: A Focus on the Protective Roles of Heme Oxygenase (HO)-1. *Front Physiol,* 10**:** 70, 2019.

111. Melber, A, Haynes, CM: UPR(mt) regulation and output: a stress response mediated by mitochondrial-nuclear communication. *Cell Res,* 28**:** 281-295, 2018.

112. Martin, J: Molecular chaperones and mitochondrial protein folding. *J Bioenerg Biomembr,* 29**:** 35-43, 1997.

113. Muz, B, de la Puente, P, Azab, F, Azab, AK: The role of hypoxia in cancer progression, angiogenesis, metastasis, and resistance to therapy. *Hypoxia (Auckl),* 3**:** 83-92, 2015.

114. Behroozian, A, Beckman, JA: Microvascular Disease Increases Amputation in Patients With Peripheral Artery Disease. *Arterioscler Thromb Vasc Biol,* 40**:** 534-540, 2020.

115. Khan, AUM, Torelli, A, Wolf, I, Gretz, N: AutoCellSeg: robust automatic colony forming unit (CFU)/cell analysis using adaptive image segmentation and easy-to-use post-editing techniques. *Sci Rep,* 8**:** 7302, 2018.

116. Horev-Azaria, L, Kirkpatrick, CJ, Korenstein, R: Predictive toxicology of cobalt nanoparticles and ions: comparative in vitro study of different cellular models using methods of knowledge discovery from data. *Toxicol Sci,* 122**:** 489-501, 2011.

117. Silvestre, JS, Planat-Benard, V, Casteilla, L: Adipose tissue-derived therapeutic cells for peripheral artery diseases: the fatty blessing. *Expert Opin Biol Ther,* 16**:** 735-738, 2016.

8 APPENDIX

Table 11. List of tables used in this thesis.

Table 12. List of figures used in this thesis.

9 RESUME

PERSONAL INFORMATION

Name und Vorname: ....Zheng, Jiaxing

Geburtsdatum: 13.05.1987

Geburtsort: .... Xinjiang China

Familienstand: ....Verheiratet

Vater: ....Zheng, Xiaodong

Mutter: ....Guan, Yufen

SCHOOL EDUCATION

09.2003 – 07.2006   ....Changji No.1 Middle School

UNIVERSITY EDUCATION

09/2006 – 07/2011
Xinjian University of Medicine

Bachelor's degree (Major in Traditional Chinese Medicine)

09/2011 – 07/2014
Yangzhou University

Master's degree (Major in Traditional Chinese Medicine)

10/2017 – recently
Medical Faculty Mannheim of the University of Heidelberg

Doctor of Medicine student of Surgical research laboratory (CFL)

10 ACKNOWLEDGEMENT